HHS Public Access

Author manuscript

Curr Biol. Author manuscript; available in PMC 2023 March 24.

Published in final edited form as:

Curr Biol. 2022 January 10; 32(1): 14–25.e4. doi:10.1016/j.cub.2021.10.009.

Disparate insults relevant to schizophrenia converge on impaired spike synchrony and weaker synaptic interactions in prefrontal local circuits

Jennifer L. Zick, MD, PhD[1,2], **David A. Crowe, PhD**[3], **Rachael K. Blackman, MD, PhD**[1,2], **Kelsey Schultz**[1,6], **David W. Bergstrand**[3,7], **Adele L. DeNicola, PhD**[1,8], **Russell E. Carter, PhD**[1], **Timothy J. Ebner, MD, PhD**[1], **Lorene M. Lanier, PhD**[1], **Theoden I. Netoff, PhD**[5,9], **Matthew V. Chafee, PhD**[1,4,9,10,*]

[1]Department of Neuroscience, University of Minnesota, Minneapolis, MN, USA 55455.

[2]Medical Scientist Training Program (MD/PhD), University of Minnesota, Minneapolis, MN, USA 55455.

[3]Department of Biology, Augsburg University, Minneapolis, MN, USA 55454.

[4]Brain Sciences Center, VA Medical Center, Minneapolis, MN, USA 55417.

[5]Department of Biomedical Engineering, University of Minnesota, Minneapolis, MN, USA 55455.

[6]K.E. Schultz current address: Department of Biology, University of Oregon, Eugene, OR, USA 97403.

[7]D. W. Bergstrand current address: Department of Pediatrics, University of Wisconsin, Madison, WI, USA, 53792.

[8]A.L. DeNicola current address: Department of Neurology, University of Minnesota, Minneapolis, MN, USA 55455.

[9]Co-senior author

[10]Lead contact

SUMMARY

Schizophrenia results from hundreds of known causes, including genetic, environmental, and developmental insults that cooperatively increase risk of developing the disease. In spite of

*Correspondence: chafe001@umn.edu (M.V.C).

AUTHOR CONTRIBUTIONS

Conceptualization, J.L.Z., T.I.N., and M.V.C.; Methodology, J.L.Z., R.K.B., K. S., A.L.D., R.E.C, L.M.L, and M.V.C.; Software, J.L.Z., D.A.C., R.K.B., D.W.B, and M.V.C.; Validation, J.L.Z., and D.A.C.; Formal Analysis, J.L.Z., D.A.C., and T.I.N.; Investigation, J.L.Z., R.K.B., K.S., A.L.D., and R.E.C.; Writing-Original Draft, J.L.Z., and M.V.C. (primary); Writing-Review & Editing, J.L.Z., D.A.C., R.K.B., K.S., A.L.D., T.J.E., L.M.L., T.I.N., and M.V.C.; Visualization, J.L.Z., D.A.C., and M.V.C; Supervision, T.J.E., T.I.N. and M.V.C.; Resources, L.M.L., T.J.E., and M.V.C.; Funding Acquisition, T.I.N., and M.V.C.

DECLARATION OF INTERESTS

The authors declare no competing interests

the diversity of causal factors, schizophrenia presents with a core set of symptoms and brain abnormalities (both structural and functional) that particularly impact the prefrontal cortex. This suggests that many different causal factors leading to schizophrenia may cause prefrontal neurons and circuits to fail in fundamentally similar ways. The nature of convergent malfunctions in prefrontal circuits at the cell and synaptic levels leading to schizophrenia are not known. Here we apply convergence-guided search to identify core pathological changes in the functional properties of prefrontal circuits that lie downstream of mechanistically distinct insults relevant to the disease. We compare the impacts of blocking NMDA receptors in monkeys, and deleting a schizophrenia risk gene in mice on activity timing and effective communication in prefrontal local circuits. Although these manipulations operate through distinct molecular pathways and biological mechanisms, we found they produced convergent pathophysiological effects on prefrontal local circuits. Both manipulations reduced the frequency of synchronous (0-lag) spiking between prefrontal neurons, and weakened functional interactions between prefrontal neurons at monosynaptic lags as measured by information transfer between the neurons. The two observations may be related, as reduction in synchronous spiking between prefrontal neurons would be expected to weaken synaptic connections between them via spike-timing dependent synaptic plasticity. These data suggest that the link between spike timing and synaptic connectivity could comprise the functional vulnerability that multiple risk factors exploit to produce disease.

eTOC blurb

Zick et al compare the downstream impacts of blocking NMDAR in monkeys and deleting a schizophrenia risk gene in mice on spiking dynamics of neurons in prefrontal local circuits. They report that the two manipulations convergently reduce synchronous spiking and weaken synaptic interactions between neurons.

Keywords

Schizophrenia; genetic risk; Dgcr8; NMDA; mouse; monkey; prefrontal cortex; local circuits; cross correlation; transfer entropy

INTRODUCTION

Schizophrenia is characterized by the disrupted functional activation[1–4] and synaptic disconnection[5–7] of prefrontal cortical circuits. The biological processes that cause prefrontal circuits to fail are unknown. Many risk factors have been identified that incrementally increase risk, including a large number of genetic mutations[8–10], maternal infection[11,12], cannabis exposure[13,14], immigrant status[15], and urbanicity[16,17] among other environmental stressors. Each of these factors, or several acting in concert[18–20] can lead to the emergence of positive symptoms (hallucinations, delusions, thought disorder), negative symptoms (flatness of affect, avolition), and cognitive deficits[4,21] in adolescence. However, the biological processes that link upstream risk factors to downstream prefrontal circuit failures to produce the symptoms of schizophrenia are poorly understood. One way to identify the causal biology leading to prefrontal circuit failure in schizophrenia is convergence-guided search. This approach tracks the downstream impacts of multiple disease-relevant insults to find the common pathophysiological endpoints where multiple

causal pathways intersect. If such convergent impacts can be identified, they could identify the functional vulnerability in prefrontal circuits that many risk factors exploit to drive disease. Given the number and diversity of causal factors identified thus far, convergence-guided search may be the most efficient way to link causes to effects in pathogenesis. Importantly, convergence cannot be demonstrated in any single model or by any single experimental manipulation.

One point where schizophrenia-related insults may functionally converge is the physiological dynamics of prefrontal recurrent local circuits[22–27]. Recurrent circuits in prefrontal cortex are formed in part by a dense plexus of axon collaterals synapsing on dendritic spines of nearby pyramidal neurons[28,29]. These circuits employ distinct synaptic mechanisms[23,30], have unique architectural features[31,32] and physiological dynamics[33], and are thought to be responsible for generating persistent patterns of neuronal activation associated with working memory[23–25].

In this study, we pursue convergence-guided search to determine whether mechanistically divergent insults relevant to schizophrenia converge on a common mode of failure in prefrontal local circuits, characterized by a disruption in effective communication between neurons. Synaptic interactions between neurons leave a trace in the temporal structure of their spike trains. By analyzing this temporal structure, it is possible to recover the pattern of functional neural interactions[34–40]. Our approach is motivated by evidence that synaptic communication between neurons is likely to be disrupted in schizophrenia[5,9,41–43], and may be a core aspect of the disease. The temporal patterning of spikes in synaptically communicating neurons controls the flow of information through networks, and consequently the computations which those networks perform[44,45]. That patterning can also rewire cortical networks through spike-timing dependent synaptic plasticity[46]. Therefore, the relationship between spike timing and synaptic connectivity in prefrontal local circuits is bidirectional and likely to control not only the synaptic integrity, but also the computational integrity of those circuits.

We previously reported that blocking NDMAR in monkeys reduced synchronous (0-lag) spiking in prefrontal neurons[47,48], and also reduced effective communication between prefrontal neurons at monosynaptic lags[47]. Based on our prior study, spike asynchrony and effective disconnection could be dynamical epiphenomena unique to monkey prefrontal circuits or the impact of blocking NMDAR on these circuits (in which case, they would have limited predictive validity for humans). Alternatively, these perturbations may represent a key link in the pathogenic chain leading to disease, in which case multiple risk factors in schizophrenia ought to bring prefrontal local circuits to the same functional endpoint, characterized by spike asynchrony and functional disconnection at a cellular level. Here we provide a hard test of this prediction. We directly compare disruptions in spike timing and effective communication between neurons in prefrontal local circuits of monkeys resulting from NMDAR blockade, and in mice resulting from a genetic mutation that increases risk of schizophrenia in humans. In mice, we deleted one copy of the gene *Dgcr8*[49–52]. *Dgcr8* is located within the 22q11.2 microdeletion region[53,54], and codes for a nuclear protein critical in the biosynthesis of miRNA[55]. miRNA in turn bind to mRNA, suppressing their translation into proteins, including mRNA that code for NMDAR subunits[56]. Consistent

with the fact that miRNA negatively regulate their mRNA targets, mutations which delete *Dgcr8* lead to enhanced NMDAR-dependent synaptic actions, including enhanced LTP[57]. Consequently, blocking NMDAR pharmacologically and deleting *Dgcr8* would be expected to be mechanistically divergent producing opposite effects on NMDAR synaptic function. Here we provide evidence that the two manipulations similarly disrupt spike synchrony and weaken effective communication between neurons in prefrontal local circuits. That convergence identifies the link between spike decorrelation and synaptic disconnection as a potential tipping point in the failure of prefrontal local circuits in schizophrenia - a pathogenic waypoint through which many different pathogenic trajectories pass. If prefrontal local circuits pass through the same functional waypoint during schizophrenia pathogenesis in humans, this would highlight a new set of biological processes to target with future therapeutics. For example, interventions which broadened the temporal window in which spike timing enhanced synaptic plasticity in dendritic spines could help lessen or potentially reverse the disconnection of prefrontal local circuits in the disease.

RESULTS

To examine how schizophrenia-relevant insults alter the neural dynamics of prefrontal local circuits, we used a microdrive (Figure 1A) to advance 16 independently movable microelectrodes into the dorsolateral prefrontal cortex of monkeys (Figure 1B, C) and the medial prefrontal cortex of mice (Figure 1E). Over recording days this allowed us to accumulate data containing the spiking activity of different neural ensembles consisting of 15–30 simultaneously recorded neurons. We recorded neural activity in a resting state condition in both species (Methods). The results of this paper describe the impact of schizophrenia-relevant manipulations on spike correlation patterns in these neural ensembles.

In monkeys, we recorded the spiking activity of 1678 prefrontal neurons, with 38 ensembles of cells recorded under the Naïve condition, 16 under the Saline condition, and 35 under the Drug condition. In mice, we recorded the spiking activity of 409 neurons (215 from *Dgcr8*$^{+/-}$ animals, 194 units from WT animals), with 14 neural ensembles from 6 individual control mice and 15 ensembles from 8 individual *Dgcr8*$^{+/-}$ mutant mice.

Convergent influence on synchronous spiking

Blocking NMDAR and deleting *Dgcr8* convergently reduced spike synchrony without influencing spike rate in prefrontal local circuits. We evaluated spike synchrony in pairs of prefrontal neurons by constructing cross-correlation histograms (CCHs). CCHs count coincident spike events between a pair of neurons as a function of the temporal lag between the spikes. Since the number of spike co-occurrences expected by chance at each lag increases with the firing rates of the neurons, coincident spike counts expected by chance were estimated in a bootstrap procedure jittering spike times to preserve overall firing rates but destroy ms precision timing information (Methods). The original CCHs were bias-corrected by z-scoring counts relative to the mean and standard deviation of counts in the bootstrap distribution. Bias-corrected, population average CCHs exhibited prominent peaks at 0-lag in both monkey (Figure 2A, black) and mouse (Figure 2E, black) prefrontal

cortex, indicating that, under normal conditions, prefrontal neurons in both species tend to fire synchronous spikes more often than predicted by chance based on the neurons' firing rates. Blocking NMDAR in monkeys (Figure 2A, B; blue) and deleting *Dgcr8* in mice (Figure 2E, F; blue), reduced the height of the 0-lag peak in the population CCH. (Results of statistical tests are provided in Figure 2 and subsequent figure legends). Blocking NMDAR in monkeys (Figure 2C; blue) and deleting *Dgcr8* in mice (Figure 2G; blue) also reduced the percent of recorded neuron pairs that exhibited significant 0-lag peaks in the CCH. These changes in spike synchrony were independent of changes in spike rate both in monkeys (Figure 2D) and mice (Figure 2H). In mice, changes in spike synchrony were independent of differences in locomotion during neural recording, as neither the speed nor duration of locomotion differed between wild type and mutant mice (Figure S1).

Convergent influence on synaptically mediated interactions between neurons

Blocking NMDAR and deleting *Dgcr8* convergently weakened synaptically mediated functional interactions in prefrontal local circuits. We evaluated synaptically mediated functional interactions between prefrontal neurons in local circuits by computing transfer entropy (TE). TE analyzes temporal interdependencies in the spike trains of two neurons to determine how an action potential in one neuron alters the probability that another neuron will fire an action potential a short time later[37–40]. The results are expressed as bits of information transmitted from one neuron to the other. TE captures synaptically mediated functional interactions between neurons as confirmed both in simulated networks and spiking neuronal cultures[37–40,58–60]. Example TE functions computed from the spike trains of simultaneously recorded neuron pairs in monkey (Figure 3A, upper panel, thick black line) and mouse (Figure 3D, upper panel) prefrontal cortex exhibited peaks in transmitted information at lags below 5 ms. At the population level, TE functions peaked at a range of lags, but peaks in the 2–5 ms range were most common, consistent with a prevalence of monosynaptic interactions between the neurons[61,62], both in monkeys (Figure 3A, lower panel) and in mice (Figure 3D, lower panel). Blocking NMDAR in monkeys (Figure 3B; blue) and deleting *Dgcr8* in mice (Figure 3E; blue) significantly reduced the height of the TE peak, indicating that less information was transmitted between neurons. Similarly, blocking NMDAR in monkeys (Figure 3C; blue) and deleting *Dgcr8* in mice (Figure 3F; blue) significantly reduced the percent of neuron pairs exhibiting significant TE peaks.

Convergent influence on activity variability

Blocking NMDAR and deleting *Dgcr8* convergently decreased the variability of neural activity in monkeys and mice. We quantified the variability of neural activity by computing the Fano factor (variance/mean) of spike counts in a sequence of 50 ms time bins. The Fano factor of a homogeneous Poisson random spike process is equal to 1. In both monkeys (Figure 4A, B; black) and mice (Figure 4D, E; black), the median Fano factor was greater than 1 under control conditions. A Fano factor >1 indicates that the variance of spike counts over time bins is greater than predicted by a homogeneous Poisson process and that the firing rates of the neurons are modulated over time (perhaps by functional interactions between the neurons). Fano factors were more positively skewed in monkeys than in mice (Figure 4A, D), suggesting stronger modulations of firing rate (and neural interactions). Blocking NMDAR in monkeys (Figure 4A-C; blue) and deleting *Dgcr8* in mice (Figure

4D-F; blue) significantly reduced the Fano factor, rendering the variability of spike counts over time bins closer to that predicted by a homogenous (constant rate) Poisson process.

Convergent influence on oscillatory dynamics

Blocking NMDAR and deleting *Dgcr8* convergently reduced oscillatory power and weakened the temporal coupling of spikes to oscillations in prefrontal local circuits. We evaluated oscillatory power by performing time-frequency analysis of local field potentials (LFPs), specifically by convolving LFPs with a set of Morlet wavelets spanning the frequency range from 1 to 100 Hz[63]. We evaluated spike-field coupling by computing the pairwise phase consistency (PPC)[64] at each frequency. PPC is the average cosine of the angle between the phases of all possible pairs of spikes in a single neuron. (Values closer to +1 indicate that spikes tend to have similar phases, values closer to −1 that spikes tend to have opposite phases.) Under control conditions, power spectra in monkey and mouse prefrontal cortex exhibited elevated power (upward deviations from monotonically decreasing 1/f scaling) in the 8–30 Hz (alpha-beta) range in monkeys (Figure 5A; black), and in the 32–80 Hz (gamma) range in mice (Figure 5C; black). Blocking NMDAR in monkeys (Figure 5A; blue) and deleting *Dgcr8* in mice (Figure 5C; blue) decreased LFP oscillatory power most prominently in the alpha-beta range in monkeys, and gamma range in mice. Blocking NMDAR in monkeys (Figure 5B; blue) and deleting *Dgcr8* in mice (Figure 5D; blue) significantly weakened phase-locking between spikes and the LFP in the delta frequency range in monkeys, and delta to theta range in mice.

Persistent deficits in synchronous spiking and neural communication in monkeys

In monkeys, we recorded neural activity first in the Naive condition (before initiating the regimen of NMDAR antagonist injections). We then recorded neural activity on interleaved days following injection of either NMDAR antagonist (Drug condition), or saline (Saline condition)[47]. Analyzing neural activity during task performance, we previously reported that milder deficits in spike synchrony and neuronal communication persisted in the Saline condition once the alternating drug/saline injection sequence began[47]. (These changes were not due to the saline injections themselves, because saline injections given before first exposure to drug were without these effects[47]). In the present study, we replicate these findings in monkeys using neural activity during the gaze fixation period. As we saw previously, deficits in 0-lag spike synchrony (Figure S2A-D) and effective neuronal communication (Figure S2E, F) persisted in the Saline condition, once intermittent daily injections of NMDAR antagonist had begun. These changes in dynamics were therefore evident in resting activity and did not require engagement of prefrontal local circuits to perform computations necessary for task performance to manifest. This suggests that intermittent disruption of NMDAR synaptic transmission produces lasting changes in neuronal synchrony and communication within prefrontal local circuits (perhaps by a mechanism we detail below, Figure 6).

Relation of neural synchrony and interaction to intracortical distance

We found that the proportion of neuron pairs exhibiting significant 0-lag spike synchrony or TE coupling did not vary as a function of intracortical distance (as indexed by distance between recording electrodes) either in monkeys or mice (Figure S3). In monkeys, prefrontal

axon collaterals form a homogeneous plexus within 1 mm of their point of origin[65], and at greater distances, terminate in patchy, stripe-like zones that can extend up to 7 mm[65,66]. The finding that functional neural interactions were equiprobable in the 400–1400 μm range of electrode distances we sampled is consistent with the spatial scale of recurrent networks in prefrontal cortex.

DISCUSSION

We employed convergence-guided search, to determine whether two insults relevant to schizophrenia, operating through divergent molecular pathways and cellular mechanisms, produced convergent effects on the physiological dynamics of prefrontal local circuits. To that end, we compared the impacts of blocking NMDAR pharmacologically in monkeys[47,67], and deleting a schizophrenia risk gene (*Dgcr8*)[49,68–70] in mice, on spike timing, neuronal communication, and oscillatory dynamics in prefrontal cortex. We found that the two divergent manipulations produced convergent effects on prefrontal local circuits, including comparable and parallel reductions in: (a) 0-lag spike synchrony (Figure 2), (b) effective communication between neurons at monosynaptic lags (Figure 3), (c) spiking variability (Figure 4), (d) LFP power, and (e) spike-field coherence (Figure 5). This provides a strong test of the convergence hypothesis, suggesting that the relationship between spike timing and synaptic connectivity in prefrontal local circuits might be a functional vulnerability exploited by multiple factors leading to disease. Schizophrenia disrupts the temporal dynamics of cortical networks[22,26,71,72]. Our data builds on this work by focusing on temporal disruption of spiking activity and neuronal communication on a cellular and millisecond scale. This is the spatial and temporal scale at which activity timing and synaptic plasticity are linked[73,74]. Disruption of the link between spike timing and synaptic plasticity may be a key step causing prefrontal local circuits to fail during pathogenesis in schizophrenia.

Mechanisms of convergence

Our data do not address the mechanisms by which blocking NMDAR and deleting *Dgcr8* produce convergent downstream effects on prefrontal local circuits (rather that they do). However, it is not likely that these two manipulations converge because they produce similar immediate impacts on NMDAR synaptic function. *Dgcr8,* a gene located within the 22q11.2 microdeletion region[50], plays a critical role in the biosynthesis of miRNA that among other targets, bind to, destabilize, and suppress translation of mRNA coding for NMDAR subunits[56]. Whereas blocking NMDAR with an antagonist reduces NMDAR synaptic transmission, deleting *Dgcr8* would be expected to enhance NMDAR synaptic mechanisms. Consistent with this, antagonizing NMDAR blocks LTP[75], whereas deleting *Dgcr8* enhances LTP[57]. Thus, it is likely that the two manipulations we employed produced opposite effects on NMDAR synaptic transmission. One possible mechanism of convergence is that PFC networks may normally operate at an optimal level of NMDAR function and that either too much (*Dgcr8* deletion) or too little (NMDAR antagonist) activation of this synaptic mechanism produces a convergent pattern of disrupted activity timing in prefrontal circuits, analogous to the inverted-U dependence of prefrontal local circuits on dopamine

receptor activation[76]. Additional experiments would be needed to determine whether such a relationship holds from NMDAR mechanisms also.

It is not likely that behavioral factors either drove the differences in prefrontal neural dynamics we observed across conditions or caused downstream impacts of blocking NMDAR and deleting *Dgcr8* to converge across manipulations and species. First, in monkeys, neural activity included in the present analyses were recorded in the fixation period of the DPX cognitive control task[77]. This is a waiting period at the start of the forthcoming trial before stimuli were presented, cognitive processes engaged, or responses executed. In our prior study, we reported that task-driven changes in 0-lag spike synchrony occurred late in the trial, around the time of the motor response[47], well after the fixation period. Second, in monkeys, the current analyses were restricted to correctly performed trials. This meant that any difference in neural dynamics during the fixation period between the Naive, Saline and Drug conditions did not reflect behavioral performance on the forthcoming trial. Neural activity in prefrontal cortex can reflect choices and outcomes on previous trials in other cognitive tasks[78,79]. Since errors were more frequent in the Drug condition[47,67], the influence of choices and outcomes on prior trials could have contributed to differences in neural dynamics across conditions during the fixation period in the primate data. However, any impact on neural dynamics in the fixation period due to previous choices or outcomes would have been unique to the primate data, and likely to cause prefrontal circuit dynamics to diverge between species, rather than converge in the manner that they did. Although motor output influences cortical dynamics in mice[80], neither the speed nor duration of locomotion differed between WT and *Dgcr8* genotypes in our data (Figure S1). Therefore, differences in motor output in mice were not likely to cause the differences in prefrontal dynamics between genotypes we observed in this species.

Relation to prior studies using animal models of circuit failure in schizophrenia

Attractor states in cortical networks are patterns of activity that tend to recur over neurons as a consequence of learned synaptic connections between the neurons. As such, attractor states reflect specific patterns of correlated neural activity. Other investigators have proposed that schizophrenia involves a weakening of attractor states and hence weakening of correlated activity in cortical networks[22,81,82]. Optical imaging in mice has shown that blocking NMDAR and the 22q11.2 microdeletion both weaken attractor dynamics in primary visual cortex[22]. This provides an example of convergence between NMDAR manipulation and genetic risk in schizophrenia that is analogous to the convergence we show here. Our study extends these results by addressing neural dynamics in prefrontal rather than visual cortex, documenting cross-species translation of these dynamics between mice and monkeys, and resolving spike timing dynamics with the ms precision that links activity timing to synaptic connectivity in networks[73,74]. Extracellular recording in rat prefrontal cortex has shown that NMDAR antagonists reduce 0-lag spike synchronization[83], with differential effects depending on the chronicity of the drug administration[84–86]. Our data suggests that spike synchrony in prefrontal circuits of monkeys are similarly dependent NMDAR synaptic mechanisms (Figure 2). We previously reported that 0-lag spike correlation between prefrontal neurons increased dramatically around the time that monkeys responded and received feedback (reward) in a cognitive control task[47]. Prefrontal cortex synchronizes with

hippocampal oscillations around the time of trial feedback in other tasks[87], and blocking NMDAR weakens prefrontal oscillations encoding trial outcome at this time[88]. In the 22q11.2 mouse genetic model of schizophrenia, oscillatory synchrony between prefrontal cortex and hippocampus is disrupted[89]. These observations suggest that synchronous spiking among prefrontal neurons may reflect network oscillations at a larger scale, and that insults relevant to schizophrenia may disrupt these oscillations. We found that blocking NMDAR in monkeys and deleting *Dgcr8* in mice disrupted oscillatory dynamics in a partially convergent manner in the current study. Both manipulations reduced the power of LFP oscillations and phase coupling between spikes and LFP oscillations (Figure 5), albeit at different frequencies.

Synchrony and connectivity deficits in schizophrenia

Asynchrony [90–97], and disconnection[98] have been widely reported in schizophrenia, however whether the two aspects of the disease are mechanistically linked, that is whether asynchrony drives disconnection during pathogenesis, is not known. Disconnection is suggested by the loss of dendritic spines in prefrontal cortex[5,6,99], as well as by a reduction in functional connectivity within prefrontal networks[100–103]. We document co-occurrence of asynchrony and disconnection in prefrontal circuits at the ms and cellular scale where spike timing and synaptic plasticity are mutually interdependent[47,48,73,74]. Prefrontal neurons receive recurrent excitation via an axon collateral network linking neighboring pyramidal neurons[28,43,104]. These recurrent circuits are particularly dependent on NMDA receptors[23–25,105]. The reduction in synchronous spike correlation we observed following NMDAR blockade in monkeys could represent disruption of these local recurrent networks. That is supported by modeling studies that show recurrent networks like those in prefrontal cortex can generate 0-lag synchronous spiking[106,107]. Post-mortem studies in schizophrenia have shown that loss of dendritic spines is most pronounced in layer III of prefrontal cortex[5,43,108]. This is where the axon collateral network is particularly dense and many collateral synapses terminate[28,43,104]. It has been proposed that disruption of these connections in prefrontal circuits destabilizes patterns of activity leading to information processing deficits in schizophrenia[109]. Our data suggests a potential mechanism.

Activity-dependent disconnection of prefrontal networks in schizophrenia

In our framework[47], supported by the present data, weakened synchronous spike correlation and information transmission in prefrontal local circuits are proposed to represent a point of functional convergence downstream of multiple schizophrenia-relevant insults (Figure 6A, B). Through established spike-timing dependent plasticity mechanisms[46], reduced spike correlation could weaken synapses, further reducing spike correlation in networks, leading to further loss of synapses. Past a tipping point, this may trigger a runaway process by which spike decorrelation and synaptic disconnection drive each other in a negatively accelerating spiral leading to the disease (Figure 6C). In short, cells that do not fire together progressively unwire. The possibility that reduced NMDAR synaptic function may be one way to trigger this disconnection cycle is supported by the observations that subchronic exposure to NMDAR antagonists produces a lasting reduction in dendritic spines in monkey prefrontal cortex[110], and a lasting effective disconnection of monkey prefrontal circuits[47]. A key aspect of the model is that the runaway process driving activity-dependent disconnection

can be entered by crossing either of two thresholds in response to factors that (a) reduce synchrony (Figure 6C, upper threshold), or (b) connectivity (Figure 6C, lower threshold) in prefrontal networks until asynchrony and disconnectivity start to drive each other pushing the brain into an effective basin of attraction characterized by the synaptic disconnection of prefrontal circuits. In the present study, we found that intermittent and repeated exposure to NMDAR antagonists led to persistent reduction in neuronal communication in prefrontal local circuits (Figure S2). That suggests that disruptions in spike synchrony may lead to lasting disconnection of prefrontal local circuits. This framework accommodates the developmental time course of schizophrenia, as synaptic pruning in late adolescence[41,111] may move brain networks past a critical connectivity threshold triggering runaway activity-dependent disconnection. From this perspective, schizophrenia may represent a failure state that is actively maintained by persistent activity decorrelation in adults, and if that could be reversed, circuit disconnection may be as well. If borne out by additional experiments, this could point toward new therapeutic strategies to restore function for patients.

STAR*Methods

RESOURCE AVAILABILITY

Lead contact—Further information and requests for resources should be directed to and will be fulfilled by the lead contact, Matthew V. Chafee (chafe001@umn.edu)

Materials availability—This study did not generate new unique reagents.

EXPERIMENTAL MODEL AND SUBJECT DETAILS

Subjects—All animal care and experimental procedures conformed to National Institutes of Health (NIH) guidelines and were approved by the Institutional Animal Care and Use Committees at the University of Minnesota and Minneapolis Veterans Administration Medical Center.

Nonhuman primates—Two adult male monkeys (8–10 kg) that were individually housed were used in this study.

Mice—Fourteen male mice (8 *Dgcr8*$^{+/-}$ experimental animals and 6 *Dgcr8*$^{+/+}$ littermate wildtype controls), 3 to 5 months old, were used in this study. (Male mice were used to match the sex of the two male nonhuman primates used in a prior study[47]). *Dgcr8*$^{+/-}$ mice were generated by crossing female Nestin-Cre mice (strain: B6.Cg (SJL)-TgN(NesCre)1Kln; stock #003771) and male *Dgcr8*$^{flox/flox}$ mice (strain: B6.Cg-*Dgcr8*$^{tm1.1Blel}$/Mmjax; stock #0032051) obtained from Jackson Laboratories. In the F1 generation, 50% of the pups were functionally heterozygous for *Dgcr8* in all neuronal lineages (Dgcr8$^{flox;}$Nestin-Cre^{+}; referred to as Dgcr8$^{+/-}$ experimental animals) and 50% were heterozygous for Dgcr8^{flox}, but without Nestin-Cre (*Dgcr8*^{flox}) and phenotypically wildtype (referred to as wildtype controls)(Figure 1F). The genotype of each animal was confirmed by performing a tail biopsy at 21 days of age according to the NIH guidelines for genotyping of mice and rats using the PCR primer sequences and protocols provided by Jackson Laboratories.

METHOD DETAILS

Preparation for neural recording—Monkeys and mice were implanted with plastic recording chambers above craniotomies placed above the prefrontal cortex. Chamber implantation surgeries were conducted under general anesthesia (isoflurane gas anesthesia in monkeys, ketamine/xylazine IP injection in mice). Recording chambers were attached to screws placed in the skull using orthopedic bone cement (monkeys) or dental acrylic (mice). Postsurgical analgesia was provided with buprenorphine in both species.

NMDAR manipulation in monkeys—In monkeys, we compared neural activity under three conditions (Figure 1D): Naïve; Saline; and Drug. In the Naïve condition, we recorded neural activity before animals were first exposed to the NMDAR antagonist phencyclidine[47,48]. (On some days in the Naïve condition animals received an injection of saline.) After completing neural recording in the Naïve condition, we initiated a sequence of daily injections of either phencyclidine (Drug condition; 0.25–0.30 mg/kg i.m.), or an equivalent volume of saline (Saline condition) in approximately alternating sequence (Figure 1D)[47]. We recorded neural activity for several hours either without injection, or after injections of NMDAR antagonist or saline in order to compare spiking dynamics across experimental conditions. The Naïve and Saline conditions are differentiated based on whether the data were obtained before or after the first exposure to phencyclidine, respectively.

Neural recording—We employed a computer controlled microdrive (Figure 1A; Thomas Recording, GMbH) to independently advance 16 glass-coated platinum iridium electrodes into the prefrontal cortex of both monkeys and mice. Electrodes were spaced ~300–400 microns apart, and the electrode array was repositioned within the recording chamber over days. Electrodes were advanced individually until the spiking activity of ~10–30 individual neurons was evident above the background noise. Ensembles contained an average of 19 neurons in monkeys and 18 neurons in mice. In monkeys, the action potential waveforms of individual neurons were discriminated online (Alpha Omega Engineering Multi Spike Detector; Nazareth, Israel). The depth of each electrode was individually adjusted until waveforms of individual neurons were readily discriminable from each other and the background noise. Representative waveforms of individual neurons evident in the recorded signal of each electrode were then identified and saved as templates. A sequence of time-amplitude windows were then automatically fitted and adjusted as necessary to capture the positive and negative peaks as well as the unique shape of each neuron’s action potential waveform. Care was taken to ensure that accepted waveforms passing through the time-amplitude windows were stable and closely conforming to the templates throughout the duration of recording. In mice, spike waveforms exceeding a user adjustable trigger were saved to disk (TDT RZ2 Bioamp Processor and PZ5 Neurodigitizer) and discriminated offline using an automated clustering algorithm (MClust Spike Sorting Matlab Toolbox, version 4.3). Spike times were stored with 1 ms resolution. Both cross-correlation and transfer entropy analysis were restricted to pairs of neurons that had been recorded on different electrodes to preclude the possibility that mixing of isolated waveforms on any single electrode might bias estimates of relative spike timing between neurons. In monkeys, neural activity was recorded from Brodmann’s areas 9 and 46 in the dorsolateral prefrontal

cortex (Figure 1B, C). In mice, neural activity was recorded from the infralimbic, prelimbic, and orbital areas of the medial prefrontal cortex (Figure 1E).

Neural recording was conducted during head fixation and at rest in both species. In monkeys, neural activity was restricted to 500-ms periods during which monkeys maintained their gaze fixated on a small visual target at the center of a video monitor. The gaze fixation period occurred during the performance of the Dot Pattern Expectancy (DPX) cognitive control task[67,115] but represented a period of passive gaze fixation before presentation of informative cue and probe visual stimuli in the trial. Thus, the neural activity included in the present analysis did not include activity modulated by trial-specific stimuli or cognitive processing to determine response direction. Pre-trial fixation period activity was included on 300–400 trials of the DPX task. In mice, neural activity was recorded for 30 minutes while the mice rested or locomoted on a running wheel. During this period, their head position was fixed by attaching the cranial implant to a bar positioned above the wheel.

In both monkeys and mice, we recorded local field potentials (LFPs) along with isolated action potentials of individual neurons concurrently. LFPs were recorded at up to 4 of the 16 microelectrodes in the array. The electrode signals were sampled at 2 KHz, band-pass filtered (1–100 Hz), notch filtered (60 Hz; in monkeys), demeaned, and resampled (400 Hz) using the ft_preprocessing function of the FieldTrip open source matlab toolbox[114]. LFP channels with strong artifacts or residual 60 Hz noise were rejected.

QUANTIFICATION AND STATISTICAL ANALYSIS

Detailed results of statistical analyses are provided in the figure legends.

Cross-correlation—To determine the relative timing with which pairs of simultaneously-recorded neurons fired action potentials relative to one another, we computed cross-correlation histograms (CCHs)[35,36,47,116]. CCHs display the distribution of intervals between action potentials in each neuron pair. Raw counts of spike coincidences at each lag are expected to vary with the firing rates of the neurons. To obtain a measure of spike timing independent of firing rate, we corrected the CCHs as follows. For each neuron pair, we constructed a permutation distribution of CCHs (100 iterations) after jittering the time of each spike by a random time within the interval ± 30 ms relative to the original spike time[116]. This destroyed the precise temporal structure of the spike trains but maintained slower fluctuations in firing rate at longer time scales. We then subtracted for each neuron pair the mean count of coincident spike events at each lag in the permutation distribution from the original data. Baseline-corrected CCHs exhibited prominent peaks at 0-lag, indicative of simultaneous spiking in neuron pairs (Figure 2A, E). We considered a neuron pair to have a statistically significant 0-lag peak (Figure 2B, F) if the sum of its real CCH from lags −1 to +1 ms exceeded the 99th percentile of the distribution of this sum across permuted histograms. To compute population average CCHs, we converted counts of coincident events to z-scores using the mean and standard deviation of counts in the permutation distribution at each lag.

Transfer entropy—In addition to measuring spike timing relationships in neuron pairs using cross-correlation analysis, we focused further on identifying statistical dependencies in

the spike trains of the two neurons that were consistent with synaptic interactions between the neurons. These were cases in which an action potential in one neuron significantly impacted the probability that the other neuron in the pair would generate an action potential a short time later. For that purpose, we computed transfer entropy (TE) between neurons using an open-source Matlab toolbox developed by Ito and colleagues[38]. TE is a measure of the amount of information (in bits) the spiking activity of a 'sending' neuron transmits to the subsequent spiking activity of a 'receiving' neuron, after taking into account the spiking history of the receiving neuron. TE analysis captures causal effective interactions between neurons likely to reflect their synaptic communication (potentially through polysynaptic pathways). We computed higher-order transfer entropy (TE) from neuron J to neuron I as defined by Ito and colleagues as follows:

$$TE_{J\to I} = \sum p\left(i_{t+1}, i_t^{(k)}, j_{t+1-d}^{(l)}\right) log_2 \frac{p\left(i_{t+1} \mid i_t^{(k)}, j_{t+1-d}^{(l)}\right)}{p\left(i_{t+1} \mid i_t^{(k)}\right)}$$

The binary variables i and j represent the spiking state (1 = action potential, 0 = silent) within a given 1 ms time bin of a neuron I, defined as receiving neuron, and a neuron J, defined as sending neuron. The parameters k and l determine the number of time bins of prior spiking history of neurons I and J respectively that are considered. The parameter d specifies the lag between spike patterns in the receiving and sending neurons. We employed $k = 1$, $l = 1$, and d in the range of 1–10 ms, as in our prior report[47]. With these parameters, the analysis computed the frequency of spike patterns each consisting of a 3 element binary vector (i_{t+1}, i_t, j_{t+1-d}) describing whether the receiving neuron i spiked or not (1 or 0) in time bin $t+1$, whether the receiving neuron i spiked or not in the preceding time bin t, and whether the sending neuron j spiked or not in a preceding time bin ranging from t-9 to t. TE analysis defines the information (in bits) transmitted between neurons by counting the frequencies of the various possible spike combinations observed in the sending and receiving neuron at each lag d in the data. Based on these frequencies, the analysis then computes the conditional probability of the presence or absence of a spike in the receiving neuron as a function of the presence or absence of a spike in the sending neuron at each lag, normalized by the spiking history of the receiving neuron.

To correct for bias in TE values that may have reflected modulations in the firing rates of the neurons over time, we calculated a permutation distribution (1000 iterations) of TE functions (bits transmitted by lag) after randomly jittering the time of each spike in sending and receiving neurons ±30 ms (thereby destroying precise temporal relationships in spiking between the neurons but preserving slower modulations in firing rate). We then subtracted the mean TE function of the permutation distribution from the TE function computed using the original data, the difference between them reflecting bias (rate)-corrected transfer entropy. To determine which neuron pairs were significantly coupled (Figure 3C, F) we identified the maximum TE value for each neuron pair (from 1 to 10 ms) and compared this value to the permutation distribution at that lag. Cell pairs were considered significantly coupled if the peak in the original data exceeded the 99.9th percentile of the permutation distribution.

Burst identification—Temporal dynamics of ensembles included brief bursting periods in which many of the neurons in each ensemble exhibited elevated firing rate at the same time (Figure S4A, C). Ensemble bursts were relatively infrequent (< 10 per minute). To isolate CCH and TE estimates that were likely to reflect synaptic interactions between individual neurons in each neuron pair from these larger scale ensemble burst events, we computed CCH and TE after removing ensemble bursts from the data using an automated procedure. To detect ensemble bursts, we generated an ensemble spike density function (SDF) for each trial that was the sum of the individual neuron SDF for that trial (Figure S4A, C; blue line; 200 ms Gaussian kernel; each neuron's SDF normalized to the number of spikes in that neuron on that trial). Next, we fit a log-logistic function to the distribution of values in the single-trial ensemble SDF. We defined ensemble bursts as periods of time in which the ensemble SDF exceeded either the 90th (mouse) or 85th (monkey) percentile of the values in the log-logistic fit. These values provided the best fit between the performance of the automated algorithm and subjective estimates of accurate burst rejection based on visual inspection of the rasters of monkey and mouse activity. Bursts with an interburst interval of less than 1 s typically reflected modulation of a single burst in rasters and were joined. Once we detected periods of ensemble bursting in each trial, we removed spikes within the bursts from that trial before proceeding with cross-correlation and transfer entropy analyses. The burst rate appeared higher in mice than monkeys, but there was no significant difference between median burst rate as a function of drug condition in monkeys (Figure S4B; Kruskal-Wallis test, $p = 0.37$), or genotype in mice (Figure S4D; Kruskal-Wallis test, $p = 0.28$).

Oscillatory synchrony—We conducted spectral and time-frequency analyses of LFP by applying fast Fourier transform (FFT) and Morlet wavelet convolution using the ft_freqanalysis function in the FieldTrip Matlab toolbox[114]. We used wavelets with peak frequencies spaced in the interval of 1–100 Hz. To quantify the extent to which the timing of action potentials was phase-locked to oscillations in the LFP recordings, we computed the pairwise phase consistency (PPC) as defined by Vinck and colleagues[64]. The PPC is analogous to the phase locking value but is less sensitive to positive bias at small sample sizes (numbers of spikes)[64]. At the time of each action potential, we determined the phase of concurrently recorded LFP oscillations at each of the 20 Morlet frequencies. We used these spike time-locked phase values to compute the PPC, which is defined as the mean cosine of the angle formed between the phases of all possible pairs of spikes in a given neuron. PPC varies between −1 (if the two phase vectors in all spike pairs tend to point in opposite directions) to +1 (if the two phase vectors in all spike pairs tend to be aligned). To compute PPC, we applied the ft_spiketriggeredspectrum_stat function of the FieldTrip Matlab toolbox[114] to the spike phase data, using unweighted LFP channel averaging. Each neuronal spike train was compared to LFP signals recorded on all other electrodes in the recording. LFP data from the same electrode that the neuron was recorded from was excluded. PPC analysis of the monkey data included 960 neurons in the Naive condition and 763 neurons in the Drug condition. PPC analysis in the mouse data included 79 neurons in wildtype animals and 128 neurons in *Dgcr8* knockout animals. We subdivided neurons on the basis of whether or not they exhibited significant 0-lag coupling and computed PPC in coupled and uncoupled neurons separately. Differences in PPC between drug conditions,

genotype, or coupling status were evaluated at each of the 20 Morlet frequencies using the Mann-Whitney U test on median PPC values across all cells. Significance was evaluated at a false-discovery rate (FDR) adjusted $p < 0.05$, after applying the Benjamini-Hochberg method to correct for multiple comparisons across the 20 frequencies.

Fano factor—We quantified the variability of firing rates of each neuron over time by computing the Fano factor (variance divided by the mean) of spike counts in 50 ms bins throughout the recording session for each neuron.

Cortical distance and neural interactions—We determined whether the probability that neurons exhibited significant coupling via 0-lag CCH or TE analysis varied as a function of distance between the neurons. We computed the distance between the two electrodes (tangential to the cortical surface) on which each pair of neurons was recorded. Pairs of electrodes in the electrode array used for recording were one of eight distances apart in the range of 400–1400 μm (400, 600, 800, 900, 1000, 1100, 1200, and 1400 μm). We then determined the number of neuron pairs that were significantly coupled by CCH or TE analysis relative to all pairs recorded at each distance (Figure S3). We applied chi-squared and permutation tests to the counts of coupled/uncoupled neurons to determine whether the probability of coupling varied significantly with distance. In the permutation test we randomly shuffled the distance and coupling status of each neuron pair, and re-computed the counts of coupled neurons at each distance in the shuffled data (10,000 iterations). We rejected the null hypothesis that coupling was random with respect to distance in the case that any count of coupled pairs in the original data exceeded the 99.5th percentile of counts of coupled pairs at that distance in the shuffled data (Bonferroni corrected $p < 0.05$ across the 8 distances tested).

Data and code availability—Analyses in this paper were conducted using publicly available Matlab toolboxes (FieldTrip and TE toolbox, see Key Resources Table). Additional Matlab scripts for CCH analysis are available from the lead contact upon request.

The data for this paper is available at the open access Mendeley Data database (doi: 10.17632/y9d3yx4xj6.1 *DOI reserved but not active) at link:

https://data.mendeley.com/datasets/y9d3yx4xj6/draft?a=270d6c1c-70ec-480d-a727-a64eb7c7d24c

Any additional information required to reanalyze the data reported in this paper is available from the lead contact upon request.

Supplementary Material

Refer to Web version on PubMed Central for supplementary material.

ACKNOWLEDGEMENTS

We thank David Redish and Sophia Vinogradov for providing useful editorial comments on the manuscript. We thank Bagrat Amirikian for refinements of the CCH 0-lag and TE analysis. We thank Dean Evans for lab and project management as well as his assistance with surgeries, animal care, and neural recordings; Dale Boeff for his

assistance with neurophysiological recording system design and construction, as well as computer programming for signal processing and data analysis; Sofia Sakellaridi for her assistance with neural recordings; Aisha Mohamed for her assistance with preliminary data analysis.

Funding:

Support for this work was provided by the National Institute of Mental Health (R01MH107491 and P50MH119569 to M.V.C., 5F30MH108205-02 to J.L.Z., R25 MH101076 to R.K.B., and F31MH109238 to A.L.D.), the National Institute of General Medical Sciences (T32 GM008244 and T32 HD007151 to R.K.B. and T32GM847121 to A.L.D.), Wilfred Wetzel Graduate Fellowship (to R.K.B.), Minnesota Medical Foundation (to M.V.C. and T.I.N.), Winston and Maxine Wallin Neuroscience Discovery Fund (to M.V.C.), MnDrive Neuromodulation Fellowship (to A.L.D.).

This material is the result of work supported with resources and the use of facilities at the Minneapolis VA Health Care System. The contents do not represent the views of the U.S. Department of Veterans Affairs, the National Institutes of Health, the Department of Health and Human Services, or the United States Government.

This manuscript was prepared while RKB was employed at the University of Minnesota. The opinions expressed in this article are the author's own and do not reflect the views of the National Institutes of Health, the Department of Health and Human Services, or the United States government.

REFERENCES

1. Perlstein WM, Dixit NK, Carter CS, Noll DC, and Cohen JD (2003). Prefrontal cortex dysfunction mediates deficits in working memory and prepotent responding in schizophrenia. Biol. Psychiatry 53, 25–38. [PubMed: 12513942]
2. MacDonald AW 3rd, Carter CS, Kerns JG, Ursu S, Barch DM, Holmes AJ, Stenger VA, and Cohen JD (2005). Specificity of prefrontal dysfunction and context processing deficits to schizophrenia in never-medicated patients with first-episode psychosis. Am. J. Psychiatry 162, 475–484. [PubMed: 15741464]
3. Yoon JH, Minzenberg MJ, Ursu S, Ryan Walter BS, Wendelken C, Ragland JD, and Carter CS (2008). Association of dorsolateral prefrontal cortex dysfunction with disrupted coordinated brain activity in schizophrenia: relationship with impaired cognition, behavioral disorganization, and global function. Am. J. Psychiatry 165, 1006–1014. [PubMed: 18519527]
4. Lesh TA, Niendam TA, Minzenberg MJ, and Carter CS (2011). Cognitive control deficits in schizophrenia: mechanisms and meaning. Neuropsychopharmacology 36, 316–338. [PubMed: 20844478]
5. Glantz LA, and Lewis DA (2000). Decreased dendritic spine density on prefrontal cortical pyramidal neurons in schizophrenia. Arch. Gen. Psychiatry 57, 65–73. [PubMed: 10632234]
6. MacDonald ML, Alhassan J, Newman JT, Richard M, Gu H, Kelly RM, Sampson AR, Fish KN, Penzes P, Wills ZP, et al. (2017). Selective Loss of Smaller Spines in Schizophrenia. Am. J. Psychiatry 174, 586–594. doi: 10.1176/appi.ajp.2017.16070814. Epub 2017 Mar 31. [PubMed: 28359200]
7. Onwordi EC, Halff EF, Whitehurst T, Mansur A, Cotel M-C, Wells L, Creeney H, Bonsall D, Rogdaki M, Shatalina E, et al. (2020). Synaptic density marker SV2A is reduced in schizophrenia patients and unaffected by antipsychotics in rats. Nat. Commun. 11, 246. [PubMed: 31937764]
8. Schizophrenia_Working_Group_of_the_Psychiatric_Genomics_Consortium (2014). Biological insights from 108 schizophrenia-associated genetic loci. Nature 511, 421–7. doi: 10.1038/nature13595. Epub 2014 Jul 22. [PubMed: 25056061]
9. Fromer M, Pocklington AJ, Kavanagh DH, Williams HJ, Dwyer S, Gormley P, Georgieva L, Rees E, Palta P, Ruderfer DM, et al. (2014). De novo mutations in schizophrenia implicate synaptic networks. Nature 506, 179–84. doi: 10.1038/nature12929. Epub 2014 Jan 22. [PubMed: 24463507]
10. Dennison CA, Legge SE, Pardiñas AF, and Walters JTR (2020). Genome-wide association studies in schizophrenia: Recent advances, challenges and future perspective. Schizophr. Res. 217, 4–12. [PubMed: 31780348]
11. Brown AS, and Derkits EJ (2010). Prenatal infection and schizophrenia: a review of epidemiologic and translational studies. Am. J. Psychiatry 167, 261–280. [PubMed: 20123911]

12. Cooper SJ (1992). Schizophrenia after prenatal exposure to 1957 A2 influenza epidemic. Br. J. Psychiatry 161, 394–396. [PubMed: 1393310]
13. Di Forti M., Marconi A., Carra E., Fraietta S., Trotta A., Bonomo M., Bianconi F., Gardner-Sood P., O'Connor J., Russo M., et al. . (2015). Proportion of patients in south London with first-episode psychosis attributable to use of high potency cannabis: a case-control study. Lancet Psychiatry 2, 233–238. [PubMed: 26359901]
14. van Os J, Bak M, Hanssen M, Bijl RV, de Graaf R, and Verdoux H. (2002). Cannabis use and psychosis: a longitudinal population-based study. Am. J. Epidemiol. 156, 319–327. [PubMed: 12181101]
15. Bourque F, van der Ven E, and Malla A. (2011). A meta-analysis of the risk for psychotic disorders among first- and second-generation immigrants. Psychol. Med. 41, 897–910. [PubMed: 20663257]
16. Vassos E, Pedersen CB, Murray RM, Collier DA, and Lewis CM (2012). Metaanalysis of the association of urbanicity with schizophrenia. Schizophr. Bull. 38, 1118–1123. [PubMed: 23015685]
17. Stilo SA, and Murray RM (2019). Non-Genetic Factors in Schizophrenia. Curr. Psychiatry Rep. 21, 100. [PubMed: 31522306]
18. Clarke MC, Tanskanen A, Huttunen M, Whittaker JC, and Cannon M. (2009). Evidence for an interaction between familial liability and prenatal exposure to infection in the causation of schizophrenia. Am. J. Psychiatry 166, 1025–1030. [PubMed: 19487391]
19. Pelayo-Terán JM, Suárez-Pinilla P, Chadi N, and Crespo-Facorro B. (2012). Gene-environment interactions underlying the effect of cannabis in first episode psychosis. Curr. Pharm. Des. 18, 5024–5035. [PubMed: 22716151]
20. Fraguas D, Díaz-Caneja CM, Corripio I, González-Pinto A, Lobo A, Bioque M, Cuesta MJ, Sanjuán J, Rodríguez-Toscano E, Arias B, et al. (2017). Gene-environment interaction as a predictor of early adjustment in first episode psychosis. Schizophr. Res. 189, 196–203. [PubMed: 28262436]
21. Sheffield JM, Karcher NR, and Barch DM (2018). Cognitive Deficits in Psychotic Disorders: A Lifespan Perspective. Neuropsychol. Rev. 28, 509–533. [PubMed: 30343458]
22. Hamm JP, Peterka DS, Gogos JA, and Yuste R. (2017). Altered Cortical Ensembles in Mouse Models of Schizophrenia. Neuron 94, 153–167.e8.
23. Wang M, Yang Y, Wang C-J, Gamo NJ, Jin LE, Mazer JA, Morrison JH, Wang X-J, and Arnsten AFT (2013). NMDA receptors subserve persistent neuronal firing during working memory in dorsolateral prefrontal cortex. Neuron 77, 736–749. [PubMed: 23439125]
24. Wang XJ (1999). Synaptic basis of cortical persistent activity: the importance of NMDA receptors to working memory. J. Neurosci. 19, 9587–9603. [PubMed: 10531461]
25. Compte A, Brunel N, Goldman-Rakic PS, and Wang XJ (2000). Synaptic mechanisms and network dynamics underlying spatial working memory in a cortical network model. Cereb. Cortex 10, 910–923. [PubMed: 10982751]
26. Durstewitz D, Huys QJM, and Koppe G. (2021). Psychiatric Illnesses as Disorders of Network Dynamics. Biol Psychiatry Cogn Neurosci Neuroimaging 6, 865–876. [PubMed: 32249208]
27. Gao W-J, Yang S-S, Mack NR, and Chamberlin LA (2021). Aberrant maturation and connectivity of prefrontal cortex in schizophrenia-contribution of NMDA receptor development and hypofunction. Mol. Psychiatry.
28. González-Burgos G., Barrionuevo G., and Lewis DA. (2000). Horizontal synaptic connections in monkey prefrontal cortex: an in vitro electrophysiological study. Cereb. Cortex 10, 82–92. [PubMed: 10639398]
29. Melchitzky DS, González-Burgos G, Barrionuevo G, and Lewis DA (2001). Synaptic targets of the intrinsic axon collaterals of supragranular pyramidal neurons in monkey prefrontal cortex. J. Comp. Neurol. 430, 209–221. [PubMed: 11135257]
30. Onn S-P, Wang X-B, Lin M, and Grace AA (2006). Dopamine D1 and D4 receptor subtypes differentially modulate recurrent excitatory synapses in prefrontal cortical pyramidal neurons. Neuropsychopharmacology 31, 318–338. [PubMed: 16052247]
31. Scherzer CR, Landwehrmeyer GB, Kerner JA, Counihan TJ, Kosinski CM, Standaert DG, Daggett LP, Veliçelebi G, Penney JB, and Young AB (1998). Expression of N-methyl-D-aspartate receptor

subunit mRNAs in the human brain: hippocampus and cortex. J. Comp. Neurol. 390, 75–90. [PubMed: 9456177]

32. González-Burgos G, Miyamae T, Krimer Y, Gulchina Y, Pafundo DE, Krimer O, Bazmi H, Arion D, Enwright JF, Fish KN, et al. (2019). Distinct Properties of Layer 3 Pyramidal Neurons from Prefrontal and Parietal Areas of the Monkey Neocortex. J. Neurosci. 39, 7277–7290. [PubMed: 31341029]
33. Murray JD, Bernacchia A, Freedman DJ, Romo R, Wallis JD, Cai X, Padoa-Schioppa C, Pasternak T, Seo H, Lee D, et al. (2014). A hierarchy of intrinsic timescales across primate cortex. Nat. Neurosci. 17, 1661–1663. [PubMed: 25383900]
34. Aertsen AM, Gerstein GL, Habib MK, and Palm G. (1989). Dynamics of neuronal firing correlation: modulation of“ effective connectivity.” J. Neurophysiol. 61, 900–917. [PubMed: 2723733]
35. Perkel DH, Gerstein GL, and Moore GP (1967). Neuronal spike trains and stochastic point processes. II. Simultaneous spike trains. Biophys. J. 7, 419–440. [PubMed: 4292792]
36. Constantinidis C, Franowicz MN, and Goldman-Rakic PS (2001). Coding specificity in cortical microcircuits: a multiple-electrode analysis of primate prefrontal cortex. J. Neurosci. 21, 3646–55. [PubMed: 11331394]
37. Nigam S, Shimono M, Ito S, Yeh F-C, Timme N, Myroshnychenko M, Lapish CC, Tosi Z, Hottowy P, Smith WC, et al. (2016). Rich-Club Organization in Effective Connectivity among Cortical Neurons. J. Neurosci. 36, 670–684. [PubMed: 26791200]
38. Ito S, Hansen ME, Heiland R, Lumsdaine A, Litke AM, and Beggs JM (2011). Extending transfer entropy improves identification of effective connectivity in a spiking cortical network model. PLoS One 6, e27431. doi: 10.1371/journal.pone.0027431. Epub 2011 Nov 15.
39. Schreiber T. (2000). Measuring information transfer. Phys. Rev. Lett. 85, 461–4. [PubMed: 10991308]
40. Vicente R, Wibral M, Lindner M, and Pipa G. (2011). Transfer entropy--a model-free measure of effective connectivity for the neurosciences. J. Comput. Neurosci. 30, 45–67. doi: 10.1007/s10827-010-0262-3. Epub 2010 Aug 13. [PubMed: 20706781]
41. Sellgren CM, Gracias J, Watmuff B, Biag JD, Thanos JM, Whittredge PB, Fu T, Worringer K, Brown HE, Wang J, et al. (2019). Increased synapse elimination by microglia in schizophrenia patient-derived models of synaptic pruning. Nat. Neurosci. 22, 374–385. [PubMed: 30718903]
42. Kirov G., Pocklington AJ., Holmans P., Ivanov D., Ikeda M., Ruderfer D., Moran J., Chambert K., Toncheva D., Georgieva L., et al. . (2012). De novo CNV analysis implicates specific abnormalities of postsynaptic signalling complexes in the pathogenesis of schizophrenia. Mol. Psychiatry 17, 142–53. doi: 10.1038/mp.2011.154. Epub 2011 Nov 15. [PubMed: 22083728]
43. Hoftman GD, Datta D, and Lewis DA (2017). Layer 3 Excitatory and Inhibitory Circuitry in the Prefrontal Cortex: Developmental Trajectories and Alterations in Schizophrenia. Biol. Psychiatry 81, 862–873. [PubMed: 27455897]
44. Miller EK, Freedman DJ, and Wallis JD (2002). The prefrontal cortex: categories, concepts and cognition. Philos. Trans. R. Soc. Lond. B Biol. Sci. 357, 1123–1136. [PubMed: 12217179]
45. Neymotin SA, Jacobs KM, Fenton AA, and Lytton WW (2011). Synaptic information transfer in computer models of neocortical columns. J. Comput. Neurosci. 30, 69–84. [PubMed: 20556639]
46. Dan Y, and Poo MM (2006). Spike timing-dependent plasticity: from synapse to perception. Physiol. Rev. 86, 1033–48. [PubMed: 16816145]
47. Zick JL, Blackman RK, Crowe DA, Amirikian B, DeNicola AL, Netoff TI, and Chafee MV (2018). Blocking NMDAR Disrupts Spike Timing and Decouples Monkey Prefrontal Circuits: Implications for Activity-Dependent Disconnection in Schizophrenia. Neuron 98, 1243–1255.e5.
48. Kummerfeld E, Ma S, Blackman RK, DeNicola AL, Redish AD, Vinogradov S, Crowe DA, and Chafee MV (2020). Cognitive Control Errors in Nonhuman Primates Resembling Those in Schizophrenia Reflect Opposing Effects of NMDA Receptor Blockade on Causal Interactions Between Cells and Circuits in Prefrontal and Parietal Cortices. Biol Psychiatry Cogn Neurosci Neuroimaging 5, 705–714. [PubMed: 32513554]

49. Merico D, Costain G, Butcher NJ, Warnica W, Ogura L, Alfred SE, Brzustowicz LM, and Bassett AS (2014). MicroRNA Dysregulation, Gene Networks, and Risk for Schizophrenia in 22q11.2 Deletion Syndrome. Front. Neurol. 5, 238. [PubMed: 25484875]
50. Sellier C, Hwang VJ, Dandekar R, Durbin-Johnson B, Charlet-Berguerand N, Ander BP, Sharp FR, Angkustsiri K, Simon TJ, and Tassone F. (2014). Decreased DGCR8 expression and miRNA dysregulation in individuals with 22q11.2 deletion syndrome. PLoS One 9, e103884.
51. Stark KL, Xu B, Bagchi A, Lai W-S, Liu H, Hsu R, Wan X, Pavlidis P, Mills AA, Karayiorgou M, et al. (2008). Altered brain microRNA biogenesis contributes to phenotypic deficits in a 22q11-deletion mouse model. Nat. Genet. 40, 751–760. [PubMed: 18469815]
52. Fénelon K, Mukai J, Xu B, Hsu P-K, Drew LJ, Karayiorgou M, Fischbach GD, Macdermott AB, and Gogos JA (2011). Deficiency of Dgcr8, a gene disrupted by the 22q11.2 microdeletion, results in altered short-term plasticity in the prefrontal cortex. Proc. Natl. Acad. Sci. U. S. A. 108, 4447–4452. [PubMed: 21368174]
53. Forsyth JK, Nachun D, Gandal MJ, Geschwind DH, Anderson AE, Coppola G, and Bearden CE (2020). Synaptic and Gene Regulatory Mechanisms in Schizophrenia, Autism, and 22q11.2 Copy Number Variant-Mediated Risk for Neuropsychiatric Disorders. Biol. Psychiatry 87, 150–163. [PubMed: 31500805]
54. Merico D., Zarrei M., Costain G., Ogura L., Alipanahi B., Gazzellone MJ., Butcher NJ., Thiruvahindrapuram B., Nalpathamkalam T., Chow EWC., et al. . (2015). Whole-Genome Sequencing Suggests Schizophrenia Risk Mechanisms in Humans with 22q11.2 Deletion Syndrome. G3 5, 2453–2461. [PubMed: 26384369]
55. Guo W-T, and Wang Y. (2019). Dgcr8 knockout approaches to understand microRNA functions in vitro and in vivo. Cell. Mol. Life Sci. 76, 1697–1711. [PubMed: 30694346]
56. Corbel C, Hernandez I, Wu B, and Kosik KS (2015). Developmental attenuation of N-methyl-D-aspartate receptor subunit expression by microRNAs. Neural Dev. 10, 20. [PubMed: 26381867]
57. Earls LR, Fricke RG, Yu J, Berry RB, Baldwin LT, and Zakharenko SS (2012). Age-dependent microRNA control of synaptic plasticity in 22q11 deletion syndrome and schizophrenia. J. Neurosci. 32, 14132–14144.
58. Garofalo M, Nieus T, Massobrio P, and Martinoia S. (2009). Evaluation of the performance of information theory-based methods and cross-correlation to estimate the functional connectivity in cortical networks. PLoS One 4, e6482.
59. Orlandi JG, Stetter O, Soriano J, Geisel T, and Battaglia D. (2014). Transfer entropy reconstruction and labeling of neuronal connections from simulated calcium imaging. PLoS One 9, e98842.
60. Wibral M, Pampu N, Priesemann V, Siebenhuhner F, Seiwert H, Lindner M, Lizier JT, and Vicente R. (2013). Measuring information-transfer delays. PLoS One 8, e55809. doi: 10.1371/journal.pone.0055809. Epub 2013 Feb 28.
61. Barthó P, Hirase H, Monconduit L, Zugaro M, Harris KD, and Buzsáki G. (2004). Characterization of neocortical principal cells and interneurons by network interactions and extracellular features. J. Neurophysiol. 92, 600–608. [PubMed: 15056678]
62. English DF, McKenzie S, Evans T, Kim K, Yoon E, and Buzsáki G. (2017). Pyramidal Cell-Interneuron Circuit Architecture and Dynamics in Hippocampal Networks. Neuron 96, 505–520.e7.
63. Cohen MX (2014). Analyzing Neural Time Series Data: Theory and Practice (MIT Press).
64. Vinck M, van Wingerden M, Womelsdorf T, Fries P, and Pennartz CM (2010). The pairwise phase consistency: a bias-free measure of rhythmic neuronal synchronization. Neuroimage 51, 112–22. doi: 10.1016/j.neuroimage.2010.01.073. Epub 2010 Jan 28. [PubMed: 20114076]
65. Kritzer MF, and Goldman-Rakic PS (1995). Intrinsic circuit organization of the major layers and sublayers of the dorsolateral prefrontal cortex in the rhesus monkey. J. Comp. Neurol. 359, 131–143. [PubMed: 8557842]
66. Pucak ML, Levitt JB, Lund JS, and Lewis DA (1996). Patterns of intrinsic and associational circuitry in monkey prefrontal cortex. J. Comp. Neurol. 376, 614–630. [PubMed: 8978474]
67. Blackman RK, Macdonald AW 3rd, and Chafee MV (2013). Effects of ketamine on context-processing performance in monkeys: a new animal model of cognitive deficits in schizophrenia.

Neuropsychopharmacology 38, 2090–100. doi: 10.1038/npp.2013.118. Epub 2013 May 10. [PubMed: 23660706]

68. Rees E., Walters JT., Georgieva L., Isles AR., Chambert KD., Richards AL., Mahoney-Davies G., Legge SE., Moran JL., McCarroll SA., et al. . (2014). Analysis of copy number variations at 15 schizophrenia-associated loci. Br. J. Psychiatry 204, 108–14. doi: 10.1192/bjp.bp.113.131052. Epub 2013 Dec 5. [PubMed: 24311552]
69. Drew LJ, Crabtree GW, Markx S, Stark KL, Chaverneff F, Xu B, Mukai J, Fenelon K, Hsu P-K, Gogos JA, et al. (2011). The 22q11.2 microdeletion: fifteen years of insights into the genetic and neural complexity of psychiatric disorders. Int. J. Dev. Neurosci. 29, 259–281. [PubMed: 20920576]
70. Van L, Boot E, and Bassett AS (2017). Update on the 22q11.2 deletion syndrome and its relevance to schizophrenia. Curr. Opin. Psychiatry 30, 191–196. [PubMed: 28230630]
71. Uhlhaas PJ, and Singer W. (2010). Abnormal neural oscillations and synchrony in schizophrenia. Nat. Rev. Neurosci. 11, 100–113. [PubMed: 20087360]
72. Jadi MP, Behrens MM, and Sejnowski TJ (2016). Abnormal Gamma Oscillations in N-Methyl-D-Aspartate Receptor Hypofunction Models of Schizophrenia. Biol. Psychiatry 79, 716–726. [PubMed: 26281716]
73. Dan Y, and Poo MM (2004). Spike timing-dependent plasticity of neural circuits. Neuron 44, 23–30. [PubMed: 15450157]
74. Feldman DE (2012). The spike-timing dependence of plasticity. Neuron 75, 556–71. doi:10.1016/j.neuron.2012.08.001. [PubMed: 22920249]
75. Bliss TVP, and Collingridge GL (2013). Expression of NMDA receptor-dependent LTP in the hippocampus: bridging the divide. Mol. Brain 6, 5. [PubMed: 23339575]
76. Vijayraghavan S, Wang M, Birnbaum SG, Williams GV, and Arnsten AFT (2007). Inverted-U dopamine D1 receptor actions on prefrontal neurons engaged in working memory. Nat. Neurosci. 10, 376–384. [PubMed: 17277774]
77. Blackman RK, Crowe DA, DeNicola AL, Sakellaridi S, MacDonald AW 3rd, and Chafee MV (2016). Monkey Prefrontal Neurons Reflect Logical Operations for Cognitive Control in a Variant of the AX Continuous Performance Task (AX-CPT). J. Neurosci. 36, 4067–4079. [PubMed: 27053213]
78. Barraclough DJ, Conroy ML, and Lee D. (2004). Prefrontal cortex and decision making in a mixed-strategy game. Nat. Neurosci. 7, 404–410. [PubMed: 15004564]
79. Seo H, Barraclough DJ, and Lee D. (2007). Dynamic signals related to choices and outcomes in the dorsolateral prefrontal cortex. Cereb. Cortex 17 Suppl 1, i110–7. [PubMed: 17548802]
80. Musall S, Kaufman MT, Juavinett AL, Gluf S, and Churchland AK (2019). Singletrial neural dynamics are dominated by richly varied movements. Nat. Neurosci. 22, 1677–1686. [PubMed: 31551604]
81. Hamm JP, Shymkiv Y, Mukai J, Gogos JA, and Yuste R. (2020). Aberrant Cortical Ensembles and Schizophrenia-like Sensory Phenotypes in Setd1a+/− Mice. Biol. Psychiatry 88, 215–223. [PubMed: 32143831]
82. Zaremba JD., Diamantopoulou A., Danielson NB., Grosmark AD., Kaifosh PW., Bowler JC., Liao Z., Sparks FT., Gogos JA., and Losonczy A. (2017). Impaired hippocampal place cell dynamics in a mouse model of the 22q11.2 deletion. Nat. Neurosci. 20, 1612–1623. [PubMed: 28869582]
83. Molina LA, Skelin I, and Gruber AJ (2014). Acute NMDA receptor antagonism disrupts synchronization of action potential firing in rat prefrontal cortex. PLoS One 9, e85842. doi: 10.1371/journal.pone.0085842. eCollection 2014.
84. Young AMJ, Stubbendorff C, Valencia M, and Gerdjikov TV (2015). Disruption of medial prefrontal synchrony in the subchronic phencyclidine model of schizophrenia in rats. Neuroscience 287, 157–163. [PubMed: 25542422]
85. Dawson N, Xiao X, McDonald M, Higham DJ, Morris BJ, and Pratt JA (2014). Sustained NMDA receptor hypofunction induces compromised neural systems integration and schizophrenia-like alterations in functional brain networks. Cereb. Cortex 24, 452–464. [PubMed: 23081884]

86. Dawson N, McDonald M, Higham DJ, Morris BJ, and Pratt JA (2014). Subanesthetic ketamine treatment promotes abnormal interactions between neural subsystems and alters the properties of functional brain networks. Neuropsychopharmacology 39, 1786–1798. [PubMed: 24492765]
87. Brincat SL, and Miller EK (2015). Frequency-specific hippocampal-prefrontal interactions during associative learning. Nat. Neurosci. 18, 576–81. doi: 10.1038/nn.3954. Epub 2015 Feb 23. [PubMed: 25706471]
88. Skoblenick KJ, Womelsdorf T, and Everling S. (2016). Ketamine Alters Outcome-Related Local Field Potentials in Monkey Prefrontal Cortex. Cereb. Cortex 26, 2743–2752. [PubMed: 26045564]
89. Sigurdsson T, Stark KL, Karayiorgou M, Gogos JA, and Gordon JA (2010). Impaired hippocampal-prefrontal synchrony in a genetic mouse model of schizophrenia. Nature 464, 763–767. [PubMed: 20360742]
90. Hirvonen J, Wibral M, Palva JM, Singer W, Uhlhaas P, and Palva S. (2017). Whole-Brain Source-Reconstructed MEG-Data Reveal Reduced Long-Range Synchronization in Chronic Schizophrenia. eNeuro 4.
91. Uhlhaas PJ, and Singer W. (2015). Oscillations and neuronal dynamics in schizophrenia: the search for basic symptoms and translational opportunities. Biol. Psychiatry 77, 1001–1009. [PubMed: 25676489]
92. Uhlhaas PJ, Haenschel C, Nikolić D, and Singer W. (2008). The role of oscillations and synchrony in cortical networks and their putative relevance for the pathophysiology of schizophrenia. Schizophr. Bull. 34, 927–943. [PubMed: 18562344]
93. Mathalon DH, and Sohal VS (2015). Neural Oscillations and Synchrony in Brain Dysfunction and Neuropsychiatric Disorders: It's About Time. JAMA Psychiatry 72, 840–844. [PubMed: 26039190]
94. Sun L., Castellanos N., Grützner C., Koethe D., Rivolta D., Wibral M., Kranaster L., Singer W., Leweke MF., and Uhlhaas PJ. (2013). Evidence for dysregulated high-frequency oscillations during sensory processing in medication-naïve, first episode schizophrenia. Schizophr. Res. 150, 519–525. [PubMed: 24016727]
95. Kang SS, MacDonald AW 3rd, Chafee MV, Im C-H, Bernat EM, Davenport ND, and Sponheim SR (2018). Abnormal cortical neural synchrony during working memory in schizophrenia. Clin. Neurophysiol. 129, 210–221. [PubMed: 29197736]
96. Leicht G, Andreou C, Nafe T, Nägele F, Rauh J, Curic S, Schauer P, Schöttle D, Steinmann S, and Mulert C. (2020). Alterations of oscillatory neuronal activity during reward processing in schizophrenia. J. Psychiatr. Res. 129, 80–87. [PubMed: 32619750]
97. Shaw AD, Knight L, Freeman TCA, Williams GM, Moran RJ, Friston KJ, Walters JTR, and Singh KD (2019). Oscillatory, Computational, and Behavioral Evidence for Impaired GABAergic Inhibition in Schizophrenia. Schizophr. Bull.
98. Friston K, Brown HR, Siemerkus J, and Stephan KE (2016). The dysconnection hypothesis (2016). Schizophr. Res. 176, 83–94. [PubMed: 27450778]
99. Glausier JR, and Lewis DA (2013). Dendritic spine pathology in schizophrenia. Neuroscience 251:90–107., 10.1016/j.neuroscience.2012.04.044. Epub 2012 Apr 27. [PubMed: 22546337]
100. Lawrie SM, Buechel C, Whalley HC, Frith CD, Friston KJ, and Johnstone EC (2002). Reduced frontotemporal functional connectivity in schizophrenia associated with auditory hallucinations. Biol. Psychiatry 51, 1008–1011. [PubMed: 12062886]
101. Camchong J, MacDonald AW 3rd, Bell C, Mueller BA, and Lim KO (2011). Altered functional and anatomical connectivity in schizophrenia. Schizophr. Bull. 37, 640–650. [PubMed: 19920062]
102. O'Neill A, Mechelli A, and Bhattacharyya S. (2019). Dysconnectivity of Large-Scale Functional Networks in Early Psychosis: A Meta-analysis. Schizophr. Bull. 45, 579–590. [PubMed: 29982729]
103. Zhou Y, Zeidman P, Wu S, Razi A, Chen C, Yang L, Zou J, Wang G, Wang H, and Friston KJ (2018). Altered intrinsic and extrinsic connectivity in schizophrenia. Neuroimage Clin 17, 704–716. [PubMed: 29264112]
104. Goldman-Rakic PS (1995). Cellular basis of working memory. Neuron 14, 477–485. [PubMed: 7695894]

105. Ma L, Skoblenick K, Seamans JK, and Everling S. (2015). Ketamine-Induced Changes in the Signal and Noise of Rule Representation in Working Memory by Lateral Prefrontal Neurons. J. Neurosci. 35, 11612–11622.

106. Vicente R, Gollo LL, Mirasso CR, Fischer I, and Pipa G. (2008). Dynamical relaying can yield zero time lag neuronal synchrony despite long conduction delays. Proc. Natl. Acad. Sci. U. S. A. 105, 17157–17162.

107. Gollo LL, Mirasso C, Sporns O, and Breakspear M. (2014). Mechanisms of zero-lag synchronization in cortical motifs. PLoS Comput. Biol. 10, e1003548.

108. Kolluri N, Sun Z, Sampson AR, and Lewis DA (2005). Lamina-specific reductions in dendritic spine density in the prefrontal cortex of subjects with schizophrenia. Am. J. Psychiatry 162, 1200–2. [PubMed: 15930070]

109. Krystal JH, Anticevic A, Yang GJ, Dragoi G, Driesen NR, Wang X-J, and Murray JD (2017). Impaired Tuning of Neural Ensembles and the Pathophysiology of Schizophrenia: A Translational and Computational Neuroscience Perspective. Biol. Psychiatry 81, 874–885. [PubMed: 28434616]

110. Elsworth JD., Groman SM., Jentsch JD., Leranth C., Redmond DE Jr., Kim JD, Diano S, and Roth RH (2014). Primate phencyclidine model of schizophrenia: sex-specific effects on cognition, brain derived neurotrophic factor, spine synapses, and dopamine turnover in prefrontal cortex. Int. J. Neuropsychopharmacol. 18.

111. Sekar A, Bialas AR, de Rivera H, Davis A, Hammond TR, Kamitaki N, Tooley K, Presumey J, Baum M, Van Doren V, et al. (2016). Schizophrenia risk from complex variation of complement component 4. Nature 530, 177–83. doi: 10.1038/nature16549. Epub 2016 Jan 27. [PubMed: 26814963]

112. Kanyuch N, and Anderson S. (2017). Animal Models of Developmental Neuropathology in Schizophrenia. Schizophr. Bull. 43, 1172–1175. [PubMed: 28981858]

113. MacDonald AW 3rd (2008). Building a clinically relevant cognitive task: case study of the AX paradigm. Schizophr. Bull. 34, 619–628. [PubMed: 18487225]

114. Oostenveld R, Fries P, Maris E, and Schoffelen J-M (2011). FieldTrip: Open source software for advanced analysis of MEG, EEG, and invasive electrophysiological data. Comput. Intell. Neurosci. 2011, 156869.

115. Blackman RK, Crowe DA, DeNicola AL, Sakellaridi S, MacDonald AW 3rd, and Chafee MV (2016). Monkey Prefrontal Neurons Reflect Logical Operations for Cognitive Control in a Variant of the AX Continuous Performance Task (AX-CPT). J. Neurosci. 36, 4067–79. doi: 10.1523/JNEUROSCI.3578-15.2016. [PubMed: 27053213]

116. Fujisawa S, Amarasingham A, Harrison MT, and Buzsáki G. (2008). Behavior-dependent short-term assembly dynamics in the medial prefrontal cortex. Nat. Neurosci. 11, 823–833. [PubMed: 18516033]

Highlights

- Impacts of different schizophrenia risk factors converge on prefrontal local circuits
- Convergent downstream impacts include Impaired spike timing and synaptic interactions
- Parallel changes in prefrontal circuits occur in monkey drug and mouse genetic models
- Spike-timing dependent plasticity may disconnect prefrontal circuits in schizophrenia

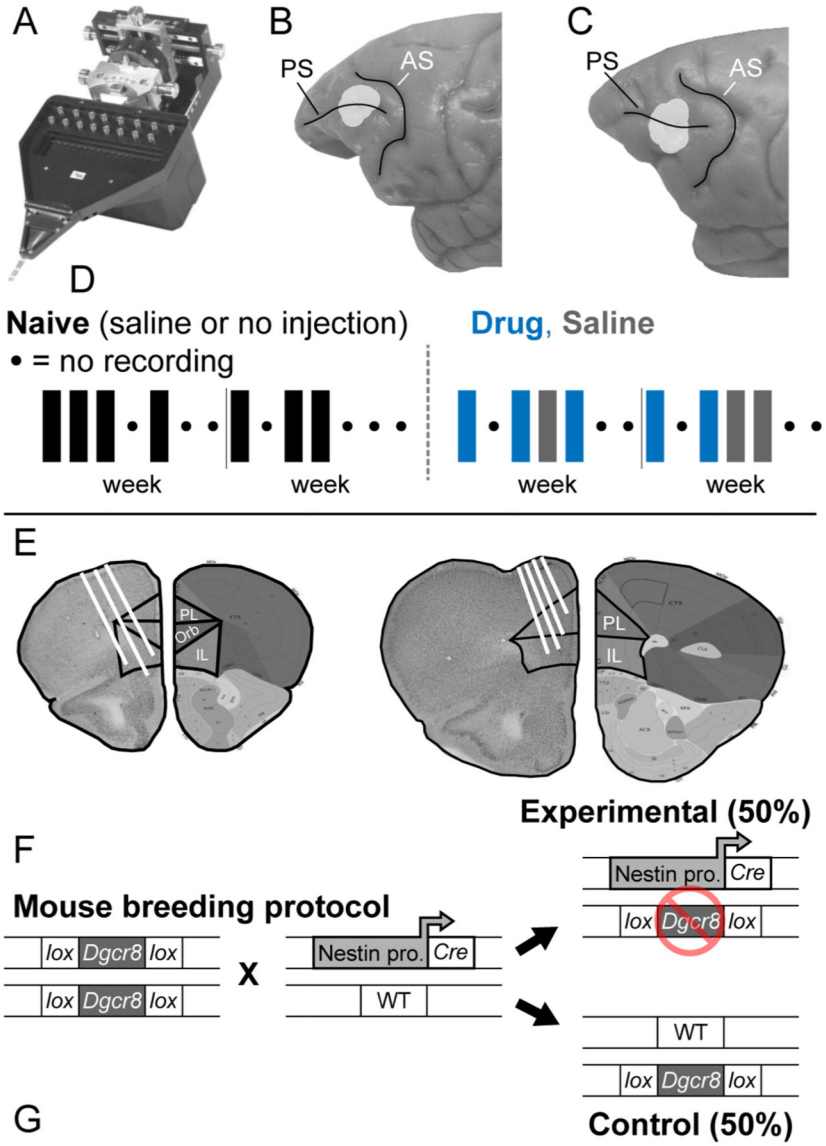

Species	Manipulation	Behavioral	Strengths	Weaknesses
Monkey	Pharmacological	Awake, resting	Face validity	Construct validity
Mouse	Genetic mutation	Awake, resting	Construct validity	Face validity

Figure 1. Experimental design.

(A) Spiking activity of small neural ensembles of individually isolated prefrontal neurons were recorded in monkeys and mice using an Eckhorn microelectrode drive (Thomas recording, GmbH) that advanced 16 thin (70 μm o.d.) glass coated platinum iridium microelectrodes independently into the brain under computer control. **(B-C)** Locations of ensemble neural recording (light gray shading) in Brodmann area 46 surrounding the principal sulcus (PS) in monkeys 1 (B) and 2 (C). **(D)** Neural recording sequence in relation to experimental conditions in monkeys. Neural activity was recorded in three conditions:

(Naïve) before first exposure to NMDAR antagonist (either with no injection or after an injection of saline), (Drug) following intramuscular, systemic injection of NMDAR antagonist (phencyclidine, 0.25–0.30 mg/kg, i.m.), and (Saline) following intramuscular injection of saline but after first exposure to NMDAR antagonist. Once neural recording in the Naïve condition was completed, daily injections of either drug or saline with neural recording afterward commenced. For a complete description of the injection sequence, see[47]. **(E)** Electrode locations in coronal slices from two representative mouse brains. The right half of each slice is an image modified from the Allen Brain Atlas (Image credit: Allen Institute). The left half of each slice is a section through prefrontal cortex at the level of neural recording, with relevant border lines between prelimbic (PC) and infralimbic (IL) prefrontal areas superimposed, and recording tracts indicated (white lines). **(F)** Mouse breeding protocol. *Nestin-Cre* heterozygous and *Dgcr8flox/flox* homozygous mice were purchased from Jackson laboratories and interbred. Experimental offspring carried the Nestin-promoter and *Cre* gene and the *Dgcr8flox* allele, resulting in the deletion of a single Dgcr8 allele in neural tissue (referred to as $Dgcr8^{+/-}$). Littermates with the *Dgcr8flox* allele but lacking *Nestin-Cre* were effectively wildtype (WT) and used as experimental controls. All genotypes were confirmed via standard tail snip genotyping protocols. **(G)** Complementary strengths and weaknesses of monkey drug and mouse genetic schizophrenia-relevant models[112]. The monkey drug model has comparatively strong face validity, because it captures cognitive behavioral deficits seen in patients with schizophrenia [67,113], but comparatively weak construct validity, because the schizophrenia-relevant manipulation is pharmacological. Conversely, the mouse genetic model has comparatively weak face validity, because of the large gap between the cognitive and behavioral capacities of mice and patients, but comparatively strong construct validity, because the schizophrenia-relevant manipulation relates to known genetic risk.

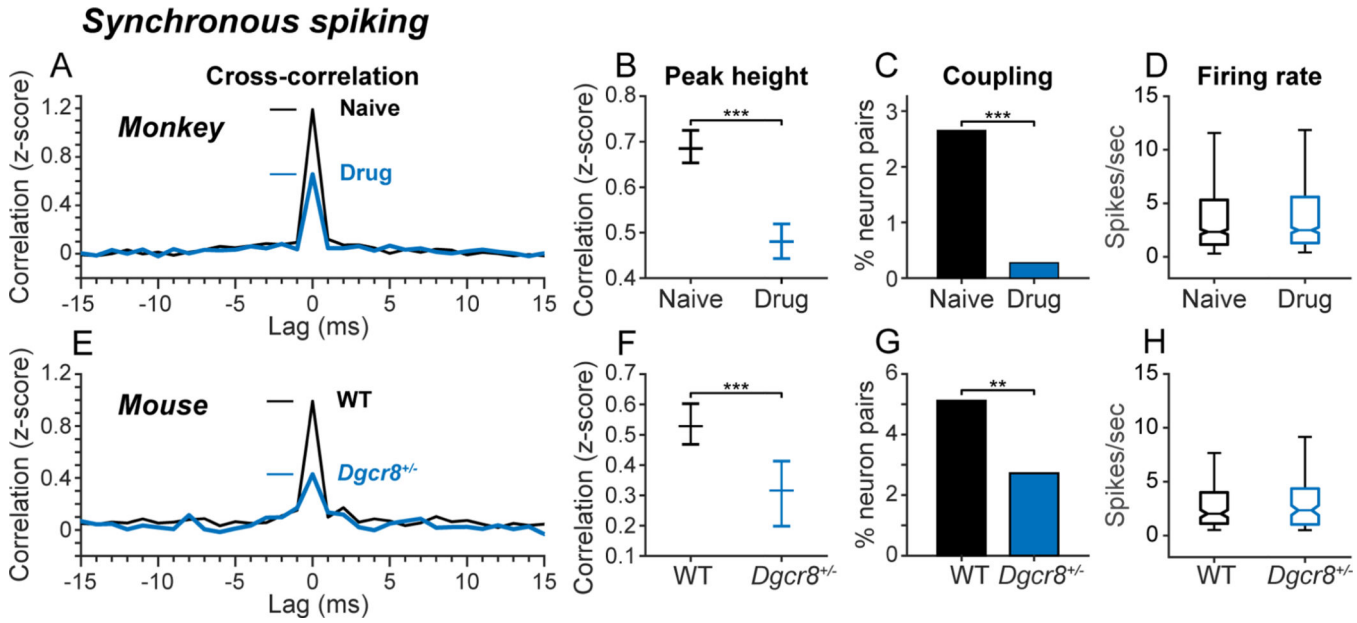

Figure 2. Convergent influence on synchronous spiking.

Influence of drug condition (A-D; monkeys) and genotype (E-H; mice) on spike correlation. **(A, E)** Population bias-corrected cross-correlation histograms (CCHs) averaged over all recorded neuron pairs as a function of drug condition in monkeys (A) and genotype in mice (E). CCH values were converted to z-scores for each neuron pair using the mean and standard deviation of permutation distribution of coincident spike counts obtained at each lag after jittering spike times in the original spike trains randomly within ± 30 ms. **(B, F)** Median (and 95% confidence interval) of z-scored 0-lag CCH peak heights across experimental conditions in monkeys (B) and mice (F). The height of the 0-lag CCH peak was significantly reduced by blocking NMDAR in monkeys (Kruskal-Wallis test, $X^2_{df=1}$ = 86.6, $p < 10^{-19}$, N_{naive} = 5080 pairs, N_{Drug} = 4180 pairs; ***$p < 0.001$) and hemizygous deletion of *Dgcr8* in mice (Kruskal-Wallis test, $X^2_{df=1}$ = 19.2, $p < 10^{-4}$, N_{WT} = 921 pairs, N_{Dgcr8} = 640 pairs; ***$p < 0.001$). **(C, G)** Percentage of simultaneously recorded pairs of neurons in monkeys (C) and mice (G) that met cutoff criteria for significant 0-lag coupling. Neuron pairs were considered significantly coupled if the height of the 0-lag peak (± 1 ms) in the CCH exceeded the 99th percentile of a permutation distribution of 0-lag peak heights in CCHs constructed after jittering spike times in the original spike trains randomly within ± 30 ms (100 iterations). The percentage of neuron pairs with significant 0-lag CCH peaks was significantly reduced by blocking NMDAR in monkeys (two-tailed z test of proportions, z = 11.07, $p < 10^{-20}$, N_{Drug} = 6165 pairs, N_{Naive} = 7,393; ***$p < 0.001$) and hemizygous deletion of *Dgcr8* in mice (two-tailed z test of proportions, WT vs *Dgcr8*$^{+/-}$, z = 2.32, $p < 0.01$, N_{Dgcr8} = 642 pairs, N_{WT} = 924 pairs; ***p < 0.01*). **(D, H)** Influence of experimental condition on neural firing rate. Box-whisker plots illustrate median (horizontal line), interquartile range (box), and range (whiskers) of firing rates in neurons as a function of drug condition in monkeys (D), and genotype in mice (H). Median firing rates did not significantly differ across experimental conditions either in monkeys (Kruskal-Wallis test, p = 0.80), or in mice (Kruskal-Wallis test, p = 0.46). Differences in synchronous spiking between experimental conditions did not reflect differences in motor output between

genotypes in mice (see Figure S1), the distance between recording electrodes within the range sampled (see Figure S3), or bursting in ensembles of neurons (see Figure S4). In monkeys, repeated exposure to NMDAR antagonist in the Drug condition was associated with a lasting reduction in synchronous spiking that persisted in the Saline condition (see Figure S2).

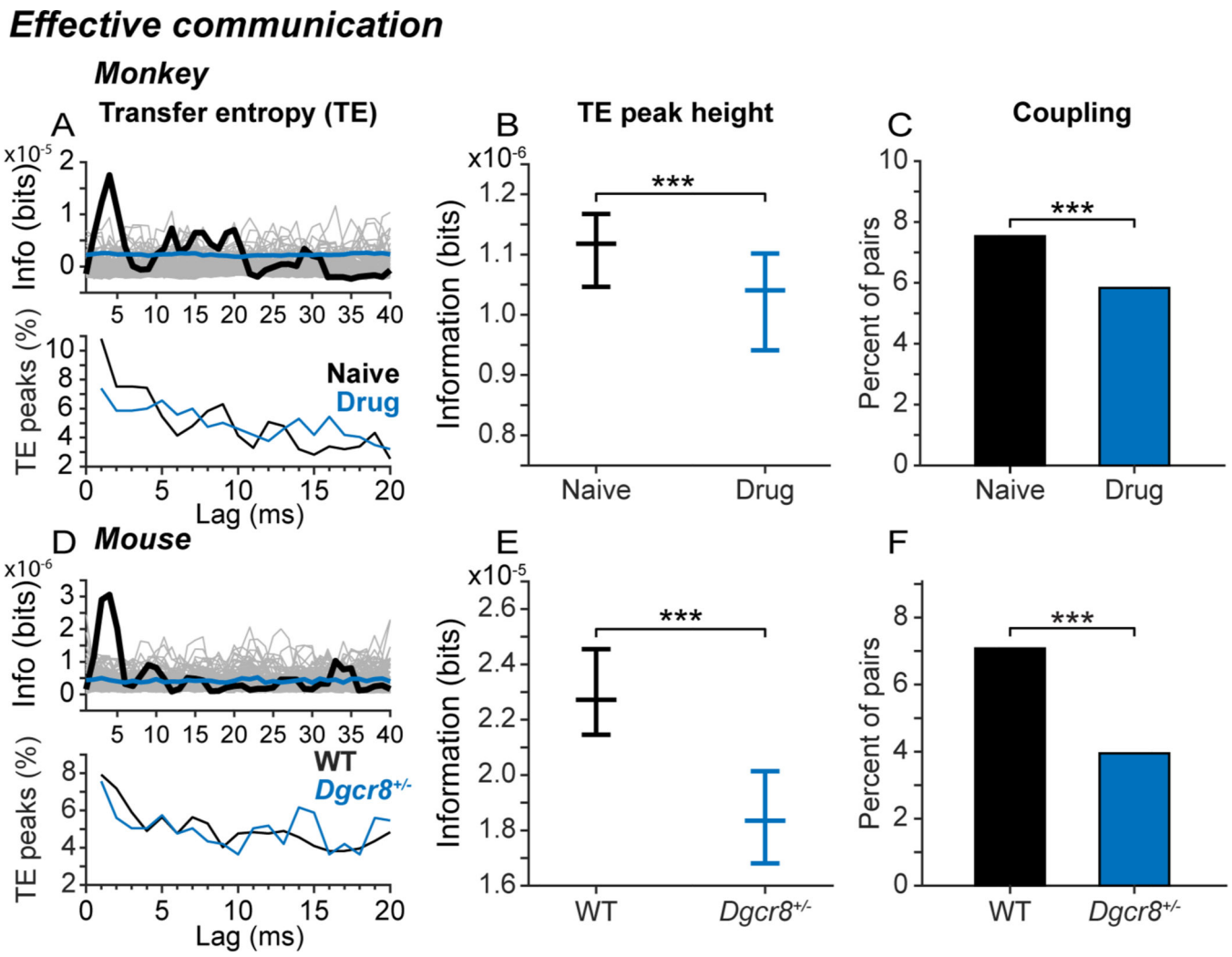

Figure 3. Convergent influence on synaptically mediated interactions between neurons.

Influence of drug condition (A-C; monkeys) and genotype (D-F; mice) on transfer entropy (TE), a measure of information transmitted between neurons based on statistical dependencies between their spike trains. **(A, D)** Example TE functions (upper panels), and distribution of lags of TE peaks (lower panels), in monkeys (A) and mice (D). In upper panels, thick black lines represent the calculated TE function over a delay of 2–40ms; grey lines represent TE functions derived from spike time-jittered bootstrap data, and blue lines represent the median of the bootstrap distribution. In lower panels, lines represent the percentage of all significant TE peaks occurring at each lag. **(B, E)** Median (and 95% confidence interval) of peak TE values across all neuron pairs in monkeys (B) and mice (E). The height of the TE peak was significantly reduced by blocking NMDAR in monkeys (Kruskal-Wallis test, $X^2_{df=1} = 18.1$, $p < 10^{-4}$, $N_{Naive} = 14{,}612$ directional pairs, $N_{Drug} = 12{,}320$ directional pairs; ***$p < 0.001$), and deleting *Dgcr8* in mice (Kruskal-Wallis test, $X^2_{df=1} = 41.72$, $p < 10^{-9}$, $N_{WT} = 2{,}004$ directional pairs, $N_{Dgcr8} = 1{,}444$ directional pairs; ***$p < 0.001$). **(C, F)** Percentage of simultaneously recorded pairs of neurons that were significantly coupled via TE analysis in monkeys (C) and mice (F). Neuron pairs were considered significantly coupled if the height of the TE peak (1–10 ms) exceeded

the 99.9th percentile of a permutation distribution of TE peaks constructed after jittering spike times in the original spike trains randomly within ± 30 ms (1000 iterations). The percentage of neuron pairs with significant TE peaks was significantly reduced by blocking NMDAR in monkeys (two-tailed z test of proportions, Naive vs Drug, $z = 5.53$, $p < 10^{-7}$, $N_{Naive} = 14{,}702$ directional pairs, $N_{Drug} = 12{,}320$ directional pairs; ***$p < 0.001$) and hemizygous deletion of *Dgcr8* in mice (two-tailed z test of proportions, WT vs *Dgcr8*$^{+/-}$, $z = 3.56$, $p < 10^{-4}$, $N_{WT} = 2{,}444$ directional pairs, $N_{Dgcr8} = 1{,}444$ directional pairs; ***$p < 0.001$). Differences in synaptically mediated neural interactions between experimental conditions did not reflect differences in motor output between genotypes in mice (see Figure S1), the distance between recording electrodes within the range sampled (see Figure S3) or bursting in ensembles of neurons (see Figure S4). In monkeys, repeated exposure to NMDAR antagonist in the Drug condition was associated with a lasting reduction in the strength of neural interactions that persisted in the Saline condition (see Figure S2).

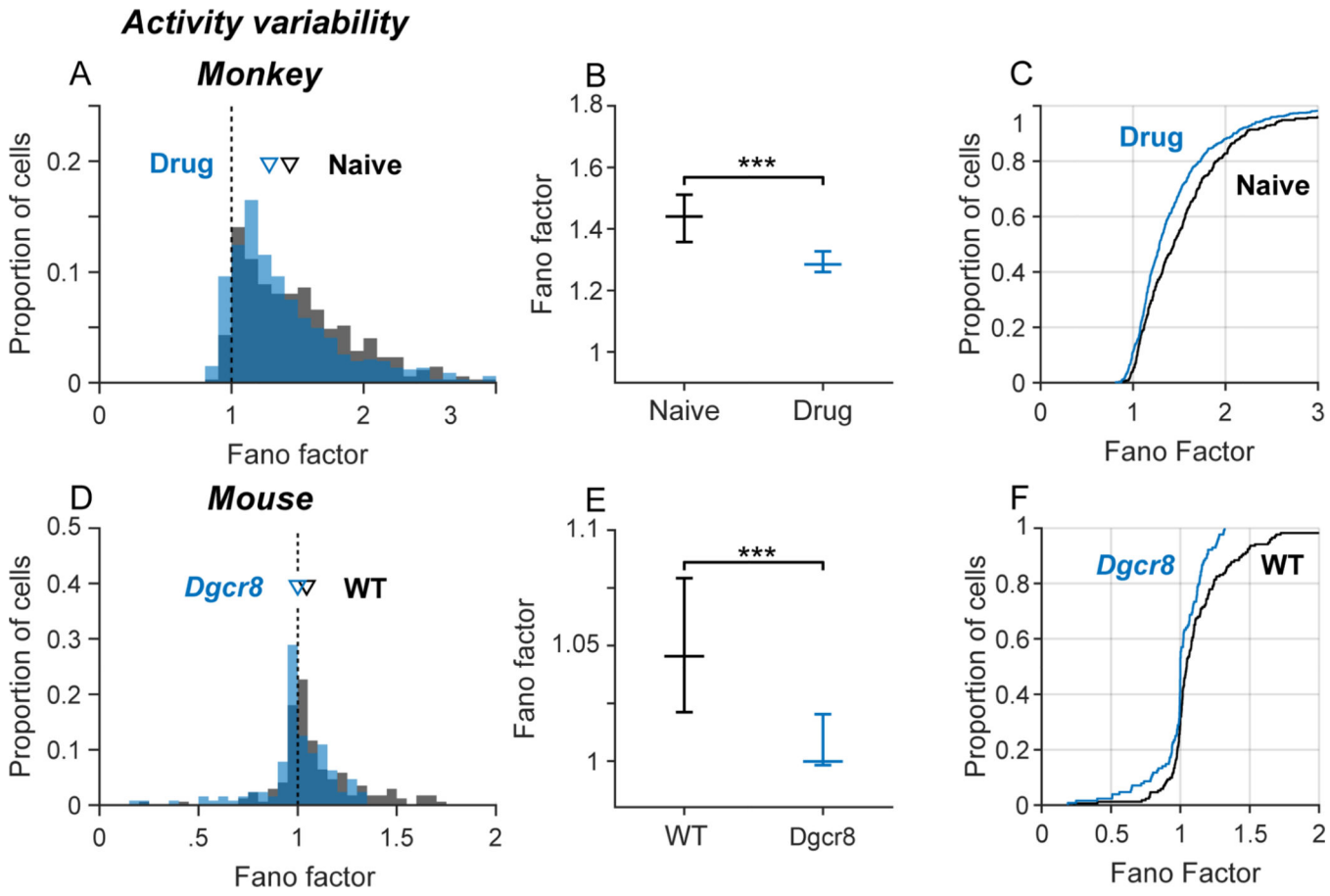

Figure 4. Convergent influence on activity variability.

Influence of drug condition (A-C; monkeys) and genotype (D-F; mice) on variability of spiking over time. Spiking variability in each neuron was quantified by the Fano factor (variance/mean) over a sequence of spike counts in 50-ms bins. **(A, D)** Frequency distribution of Fano factors by drug condition in monkeys (A) and genotype mice (D). Inverted triangles indicate population medians. **(B, E)** Median Fano factors (error bars indicate 95% confidence intervals) by drug condition in monkeys (B) and in mice (E). The Fano factor was significantly reduced by blocking NMDAR in monkeys (Kruskal-Wallis test, $X^2_{df=1} = 17.8$, $p < 10^{-4}$; ***$p < 0.001$) and hemizygous deletion of *Dgcr8* in mice (Kruskal-Wallis test, $X^2_{df=1} = 12.0$, $p < 10^{-3}$; ***$p < 0.001$). **(C, F)** Cumulative distributions of Fano factor values by drug condition in monkeys (C) and genotype mice (F). Cumulative distributions were shifted left toward smaller values by blocking NMDAR in monkeys (Kolmogorov-Smirnov test, $K = 0.15$, $p < 10^{-4}$) and hemizygous deletion of *Dgcr8* in mice (Kolmogorov-Smirnov test, $K = 0.24$, $p < 10^{-3}$).

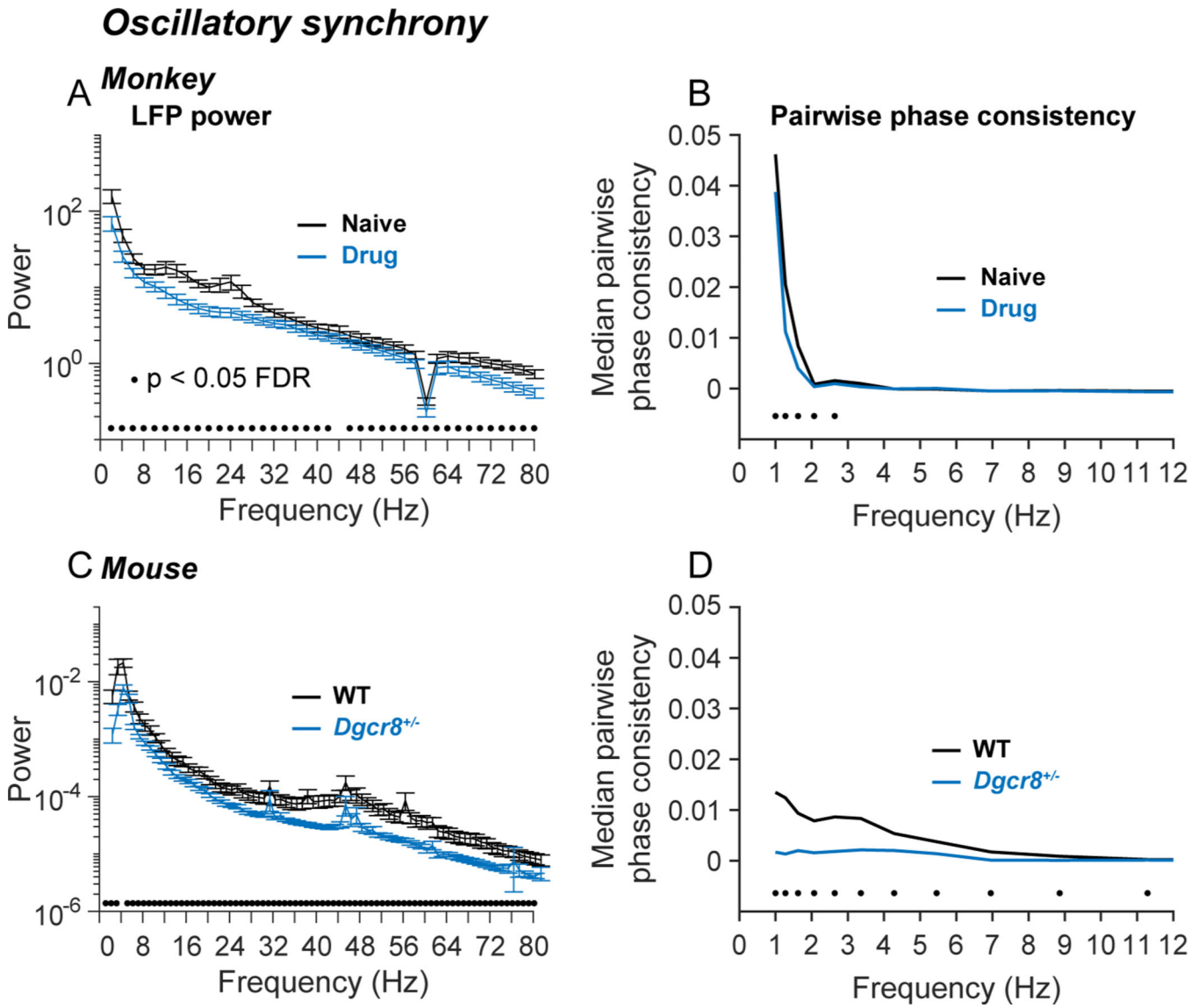

Figure 5. Convergent influence on oscillatory dynamics.

Influence of drug condition (A, B; monkeys) and genotype (C, D; mice) on LFP power (A, C) and pairwise phase consistency (PPC) between spikes and LFPs (B, D). LFP signals were convolved with a set of complex Morlet wavelets in the frequency range of 1–100 Hz using the Matlab FieldTrip[114] toolbox. After assigning phase angles to each spike (relative to LFP oscillations at a given frequency), PPC is defined as the mean cosine between the phase angles of all possible pairs of spikes, capturing the tendency for spikes to occur at consistent phases of LFP oscillations[64]. **(A, C)** Mean LFP power spectra in monkeys (A) and mice (C). LFP power was significantly reduced by blocking NMDAR in monkeys and hemizygous deletion of *Dgcr8* in mice (black dots above horizontal axis indicate $p < 0.05$ between conditions by t-test at each frequency, FDR corrected for the number of tests using the Benjamini-Hochberg method). Error bars indicate SEM over LFP channels (electrodes). The dip at 60 Hz in the monkey power spectra reflects notch filtering. **(B, D)** Median PPC as a function of frequency in monkeys (B) and mice (D). PPC was significantly

reduced by blocking NMDAR in monkeys (N_{Saline} = 960 neurons, N_{Drug}= 763 neurons) and hemizygous deletion of *Dgcr8* in mice (N_{WT} = 79 neurons, N_{Dgcr8} = 128 neurons) (black dots above horizontal axis indicate $p < 0.05$ between conditions by Wilcoxon Rank Sum test at each frequency, FDR corrected for the number of tests using the Benjamini-Hochberg method).

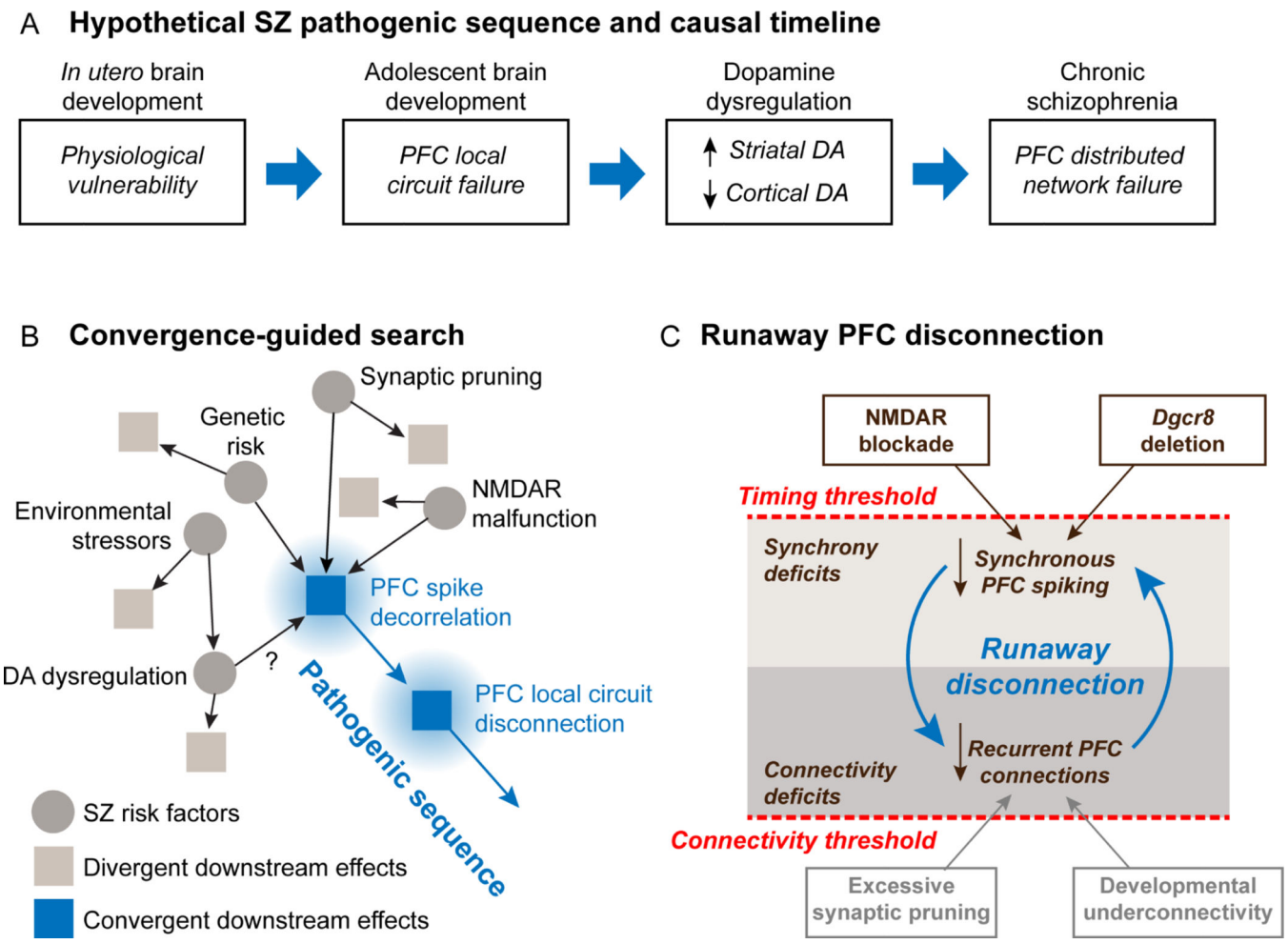

Figure 6. Convergence-guided search for causal factors in schizophrenia pathogenesis.

(A) Hypothetical pathogenic sequence leading to schizophrenia. Four stages of pathogenesis are envisioned to form a timeline leading to emergence of symptoms. The present study focuses on failure of prefrontal local circuits. (B) Convergence-guided search for causal factors in schizophrenia pathogenesis. A diversity of risk factors and insults convergently reduce temporal spike correlation, with follow-on activity-dependent disconnection of prefrontal local circuits. The present study documents convergent effects of NMDAR malfunction and genetic risk on spike decorrelation and functional uncoupling. (C) Activity-dependent disconnection. In this model, reduced spike synchrony and effective disconnection of prefrontal circuits are causally linked. If spike synchrony becomes too weak in prefrontal networks, or synaptic connections become too few, additional asynchrony and disconnection start to drive each other in a negatively accelerating spiral producing runaway activity-dependent disconnection.

KEY RESOURCES TABLE

REAGENT or RESOURCE	SOURCE	IDENTIFIER
Chemicals, peptides, and recombinant proteins		
Phencyclidine hydrochloride	Sigma-Aldrich	P3029
Experimental models: Organisms/strains		
Rhesus macaque (Macaca mulatta)	N/A	N/A
Mouse: Nestin-Cre mice (strain: B6.Cg (SJL)-TgN(NesCre)1Kln)	Jackson Labs	Stock #003771
Mouse: Dgcr8flox/flox mice (strain: B6.Cg-Dgcr8tm1.1Blel/Mmjax;)	Jackson Labs	Stock #0032051
Deposited data		
NHP and mouse spiking and LFP data	This study	https://data.mendeley.com/datasets/y9d3yx4xj6/draft?a=270d6c1c-70ec-480d-a727-a64eb7c7d24c
Software and algorithms		
MATLAB	MathWorks	RRID:SCR_001622
Transfer entropy Matlab Toolbox[38]	https://code.google.com/archive/p/transfer-entropy-toolbox/	N/A
FieldTrip Matlab Toolbox[114]	https://www.fieldtriptoolbox.org/download.php	RRID:SCR_004849